nanomaterials

MDPI

Review

Recent Advances in TiO_2-Based Photocatalysts for Efficient Water Splitting to Hydrogen

Muhammad Nisar [1,2,*], Niqab Khan [3], Muhammad I. Qadir [4] and Zeban Shah [5]

[1] Departamento de Ingeniería Eléctrica, Facultad de Ingeniería, Universidad Católica de la Santísima Concepción, Alonso de Ribera 2850, Concepción 4070129, Chile
[2] Centro de Energía, Universidad Católica de la Santísima Concepción, Alonso de Ribera 2850, Concepción 4070129, Chile
[3] São Carlos Institute of Physics, University of São Paulo (USP), P.O. Box 369, São Carlos 13560-970, SP, Brazil
[4] Instituto de Química, Universidade Federal de Goiás (UFG), Avenida Esperança s/n, Câmpus Samambaia, Goiânia 74690-900, GO, Brazil
[5] Institute of Chemistry, Federal University of Rio Grande do Sul, Av. Bento Gonçalves 9500, Porto Alegre 91501-970, RS, Brazil
* Correspondence: mnisar@ucsc.cl

Abstract

Titanium dioxide (TiO_2) has been widely used as a potential candidate for the production of green hydrogen using the artificial photosynthesis approach. However, the wide bandgap (~3.3 eV) of anatase TiO_2 makes it difficult to absorb a large fraction of the solar radiation reaching the Earth, thus providing a low photocatalytic activity. Anatase TiO_2 absorbs only 4% of solar radiation, which can be improved by engineering its bandgap to enhance absorption in the visible region. In the literature, many strategies have been adopted to improve the photocatalytic activity of TiO_2, such as metal and non-metal doping and heterojunctions. These techniques have shown incredible enhancement in visible light absorption and improved photocatalytic activity due to their ability to lower the bandgap of pure TiO_2 semiconductors. This review highlights different techniques like doping, heterojunctions, acidic modification, creating oxygen vacancies, and temperature- and pressure-dependence, which have improved the photochemical response of TiO_2 by improving charge-transfer efficiencies. Additionally, the charge-transfer mechanism and enhancement in the photochemical response of TiO_2 is discussed in each portion separately.

Keywords: titanium dioxide (TiO_2); solar energy; hydrogen production; doping and heterojunction

Academic Editor: Vincenzo Vaiano

Received: 14 May 2025
Revised: 16 June 2025
Accepted: 19 June 2025
Published: 25 June 2025

Citation: Nisar, M.; Khan, N.; Qadir, M.I.; Shah, Z. Recent Advances in TiO_2-Based Photocatalysts for Efficient Water Splitting to Hydrogen. *Nanomaterials* **2025**, *15*, 984. https://doi.org/10.3390/nano15130984

1. Introduction

Environmental pollution caused by the burning of fossil fuels has become an important challenge to tackle. The burning of fossil fuels leads to CO_2 emissions, which consequently cause the greenhouse effect. The solar energy that strikes the Earth each hour is higher than all the energy consumed by humans in a year. The conversion of solar energy to another form can suppress these environmental issues caused by fossil fuels; however, it is a huge challenge for researchers to develop devices that utilize solar energy and convert it into other forms of energy [1]. The enormous demand for global energy is becoming a major concern for the scientific community. According to a 2013 report, the worldwide energy consumption was 17 terawatts (TW, equal to 10^{12} j/s) and will be double that by 2050, and subsequently triple by 2100 [2,3]. The increase in energy demand is significantly influenced

by the growing global population, which is expected to reach approximately 9.9 billion by 2050, representing a 25% increase from the current 2023 population of 8.0 billion [4]. In addition, the increase in industrialization in recent years has also led to a high energy consumption and high demand for the Earth's limited fossil fuel reserves which has increased the amount of CO_2 discharge. The use of fossil fuels as an energy source has become one of the primary environmental issues of the 21st century. According to a report on climate change, CO_2 emissions will increase to 590 ppm by the end of the 21st century. This excessive increase in CO_2 levels could cause the Earth's temperature to rise by up to 1.9 °C, leading to other damaging effects such as increased surface water levels and more frequent extreme weather events [5–8]. It is critical to find safe, Earth-abundant, sustainable, renewable, and clean energy resources to address these energy and environmental issues [9]. Several available renewable resources are safer, cleaner, contamination-free, and sustainable compared to fossil fuels, including wind, geothermal heat, and sunlight. However, each of these renewable energy resources has its restrictions; for instance, the expensive and harmful nature of hydropower generation from a dam, the difficulty of storing the electricity generated from wind, and the high operational cost of geothermal resources make it difficult to replace the currently used non-renewable energy resources [5]. In this scenario, hydrogen can be considered as an abundant and green renewable energy source that can solve the emission problems of dangerous greenhouse gases (CO_2, CO, CH_4), which are the primary source of global climate change [10]. The energy density of hydrogen is 143 $MJkg^{-1}$, and this gas is a carbon-free energy carrier [11]. Using solar energy conversion to create clean and sustainable energy (green H_2) by water splitting and transforming it to electric power through fuel cells is a key solution to worldwide energy concerns [3,12]. Additionally, the practical confines of the introduction of a cost-effective, energy-efficient photocatalytic system for water splitting is a major dispute that needs to be resolved for the successful achievement of a solar fuel-based economy [13].

Thus far, three important methods have been established for hydrogen production, comprising electrochemical, photochemical, and solar energy-assisted thermochemical methods [14]. The basis of the thermochemical technique is the application of concentrated solar radiation to act as a driving force to split water molecules; this is considered an important technology for ecological hydrogen production as a process in future energy structures [15]. Conceptually, the ideal simple process of "water thermolysis" comprises a one-step thermal decomposition of water, where solar energy is concentrated directly on chemical reactors to separate water into hydrogen and oxygen. However, the process has some limitations, as it requires an elevated temperature above 2500 K to ensure a realistic degree of decomposition and needs a good operational H_2/O_2 separation performance to hinder the recombination of these elements; thus, direct water splitting is not recommended [14]. Photocatalytic or photochemical water splitting is a process that utilizes light energy from the Sun to split water molecules into hydrogen and oxygen. In this process, a semiconductor serves as a photocatalyst, which in the presence of UV light or visible light splits water into pure oxygen and hydrogen. The photocatalyst absorbs photons and generates electron–hole pairs that drive the redox reaction. This sustainable method provides a green way to produce hydrogen, which can be further stored and converted to another form of energy [16,17]. Recently, several catalytically active semiconductors for photochemical reactions have been developed, but a stable material that shows worthy repeatability for visible light is yet to be introduced, and its discovery is still under investigation. Thus, for water splitting, it is imperative to develop suitable materials that can satisfy three main conditions: (i) show an outstanding stability in photochemical reactions; (ii) have a lower bandgap value than 3 eV; (iii) have an appropriate band edge potential for water splitting reactions [18].

Since the pioneering discovery by Fujishima and Honda in the 1970s, numerous strategies have been developed to enhance the efficiency of photocatalytic hydrogen production [19]. In the last few decades, the exploration for the ideal materials to act as single photocatalysts has been a hot topic of research. Figure 1 illustrates a single photocatalytic system for water splitting using a semiconductor material. When irradiated with photons having energy equal to or greater than the bandgap, electrons in the valence band are excited to the conduction band, leaving behind positive holes in the valence band. The positive Gibbs free energy change (ΔG° = 237.13 kJ/mol) is a critical factor in overall water splitting, indicating that the reaction is non-spontaneous under standard conditions [20]. The strong reduction and oxidation potentials of photogenerated electrons and holes can drive redox reactions on the catalytic surface [21]. During the water splitting process, the formation of one molecule of H_2 requires two electrons, whereas the formation of one molecule of O_2 requires four holes. Therefore, the selection of a suitable semiconductor for effective water splitting primarily depends on the bandgap size, the position of the conduction band minimum (which must be more negative than the reduction potential), and the valence band maximum (which must be more positive than the oxidation potential). On the other hand, noble metals [22], enzymes, polyoxometalates (POMs), inorganic compounds, and organometallic complexes have been investigated as catalytic materials for electrochemical and photochemical H_2 production from water. An especially interesting approach involves the use of metal–organic frameworks (MOFs) in aqueous solutions or in mixtures of water and organic solvents for photochemical water reduction and oxidation [23–25].

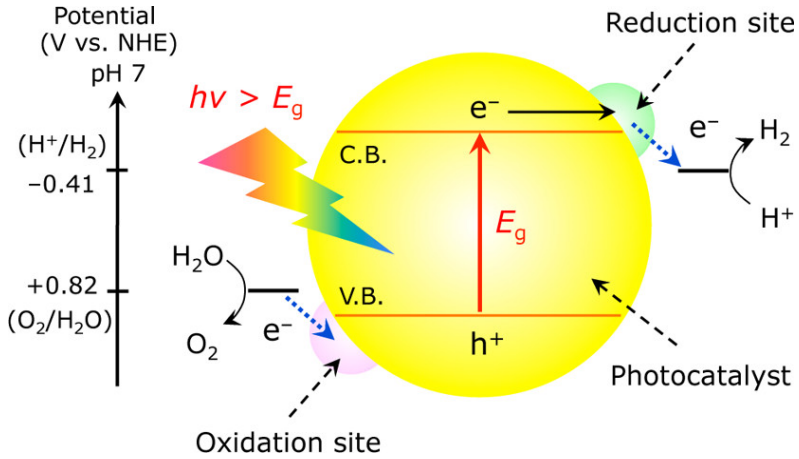

Figure 1. A typical model for photochemical water splitting, reproduced from Ref. [26], copyright 2013 American Chemical Society.

Different types of catalysts offer distinct advantages and disadvantages for chemical reactions. In the case of hydrogen production, both homogeneous and heterogeneous synthetic catalysts exhibit lower activity compared to hydrogenase enzymes. However, the practical use of hydrogenase is limited by its sensitivity to oxygen, high cultivation costs, and challenges in enzyme isolation, making it unsuitable for large-scale hydrogen production. To improve efficiency, noble metals such as platinum (Pt), palladium (Pd), and rhodium (Rh) have been loaded onto semiconductor materials. Although these metals enhance hydrogen production, their limited availability and high cost hinder their widespread use in large-scale photocatalytic fuel cells [27–29]. Considering factors such as simplicity, efficiency, cost-effectiveness, and environmental sustainability, photocatalytic water splitting is regarded as a promising method for hydrogen production. Generally, photocatalytic water splitting can be categorized into two main types: (a) photocatalytic (PC) or photochemical processes, and (b) photoelectrochemical (PEC) processes [30].

2. Photochemical Reaction

In photochemical reactions, light energy is directly utilized to initiate fundamental chemical transformations. This process typically relies on a powdered semiconductor photocatalyst that absorbs sunlight to generate electron–hole pairs, which subsequently drive the redox reactions involved in water splitting. Key factors influencing photocatalytic hydrogen production include the bandgap of the photocatalyst, surface area, efficiency of charge carrier separation, and stability under illumination. Studies have shown that, in photochemical systems, photocatalysts are commonly used as suspended particles within the reaction solution [30,31]. The authors highlighted several challenges in controlling key factors during the process, such as light absorption by suspended particles, pH fluctuations, and accurate determination of substrate concentration. These variables significantly influence the reaction kinetics, making the interpretation of experimental results difficult. Furthermore, conducting kinetic studies in suspension systems is often very time-consuming.

3. Basics of Photochemical Water Splitting

The working principle of photochemical water splitting may be described completely in four main steps as illustrated in Figure 2: (I) absorption of incoming light to produce electron–hole pairs when its energy is equal or greater than the bandgap energy of the photocatalysts; (II) separation of excited electron–hole pairs; (III) transfer of electron–hole to the surface of photocatalysts; and (IV) redox surface reaction by these charges. During the third step, a significant portion of electron–hole pairs recombines on the surface site, releasing energy in the form of heat or light. Only the long-lived photogenerated charges have the potential to participate in the surface redox reactions, and their activity depends on the donor and accepter properties of the surface-adsorbed species [32].

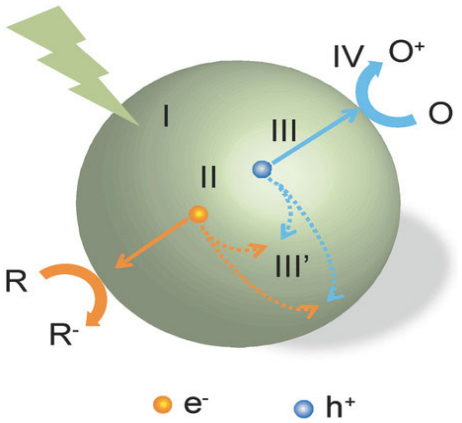

Figure 2. Steps involved in the photochemical reaction process [32].

4. Photoelectrochemical Reaction

The photoelectrochemical (PEC) reaction is a specialized form of photochemical reaction in which an external electric circuit facilitates the chemical reaction. In a PEC cell, a photocatalyst is deposited as a thin film on a conductive substrate to form a photoanode or photoelectrode, which is then immersed in an electrolyte solution to perform water splitting [30]. Hydrogen production in this system is enabled by the external circuit, which directs the photoinduced electrons from the photoanode to the photocathode. During water splitting, hydrogen and oxygen are produced simultaneously: the photogenerated electrons reduce protons at the photocathode to form hydrogen molecules, while oxygen is generated at the photoanode via water oxidation [33].

5. The Basic Concept Involves in PEC Water Splitting

Photoelectrochemical (PEC) water splitting is a complex process. Its fundamental principle involves applying an external bias to a photovoltaic or photoelectrode system immersed in an electrolyte containing redox couples. One of the electrodes is a semiconductor capable of absorbing light. Semiconductors have the unique ability to act as photocatalysts: when exposed to light, they generate electron–hole pairs that drive oxidation and reduction reactions. In PEC water splitting, the process of water electrolysis is assisted by both light and electricity. The photocatalytic electrodes absorb photons and provide the energy required for the redox reactions, while the externally applied electric or chemical bias supplies the additional voltage needed to overcome reaction barriers [34]. This external bias plays a crucial role in initiating and sustaining the reaction at a practical rate by overcoming the slow kinetics of charge transfer. Upon photon absorption, electrons are excited and electron–hole pairs are formed on the photoelectrode. The holes participate in oxidation reactions, while the excited electrons reduce protons (H^+) to produce hydrogen gas (H_2) [35,36].

On the other hand, several physical phenomena must be optimized in the design of an efficient device for photochemical water splitting, such as the interaction of light with matter. Three different phenomena—absorption, reflection, and transmission—can take place when light strikes a material's surface. The extent to which light is absorbed or reflected depends on the properties of the medium; in media such as liquid electrolytes, only slight absorption or reflection typically occurs. Thus, minimizing the light propagation distance is recommended to reduce energy losses. Once the photon is absorbed inside the material, if its energy exceeds the bandgap of the semiconductor, it can excite an electron from the valence band to the conduction band, creating an electron–hole pair. The penetration depth—which refers to the depth at which photons are absorbed within the material—is an essential criterion for thin-film semiconductors.

The excitation of electrons to higher energy levels is accomplished through the absorption of photons. In a semiconductor, the overall distribution of electronic energy states arises from the individual atomic states, forming the valence band and the conduction band. The valence band edge (Ev) is the highest occupied energy level, and the conduction band edge (Ec) is the lowest unoccupied energy level; the difference between these two edges is called the bandgap (Eg). The classification of a semiconductor as n-type or p-type depends on the position of the Fermi level (the average energy of the electronic states) relative to the valence or conduction band. A p-type semiconductor is formed if the Fermi level is close to the valence band and the majority carriers are holes, whereas, if the majority carriers are electrons and the Fermi level is close to the conduction band, an n-type semiconductor is achieved.

One of the key phenomena, "charge separation and transport," needs to be optimized for efficient material performance. The ultimate separation of light-induced electron–hole pairs is essential, as their premature recombination significantly limits the extraction of photocurrent. Thus, to generate a usable photovoltage and photocurrent, an external potential can be applied to drive the spontaneous separation of photogenerated charges. In designing a p-n junction, p-type and n-type semiconductors are brought into contact, and to reach equilibrium, free electrons and holes diffuse across the junction, resulting in a redistribution of charge. This results in the formation of a space–charge region, where a strong internal electric field is established. The electric field drives electrons and holes in opposite directions. High conductivity is crucial for efficient charge transport, and it depends on both carrier mobility and concentration.

Similarly, chemical reactions occur when photogenerated holes or electrons reach the surface of the photon-absorbing material. Water splitting involves either hydrogen

or oxygen evolution reactions; therefore, in addition to charge separation and transport, the efficiency of the reaction and the mechanism of electron transfer from reactants to products is important. The role of the catalyst in accelerating the chemical reaction is vital. Electrolytes without significant depletion steadily support electrochemical reactions while the introduction of a catalyst lowers the activation energy by providing an alternative reaction pathway, often through the formation of intermediate species on the catalyst surface. Only a small amount of catalyst is required, as the reaction takes place on the surface [37]. Below are the equations describing the general photoelectrochemical water-splitting mechanism [34].

$$2H_2O + h\nu \rightarrow 2H_2 + O_2\ \Delta G^\circ = 4.92\ Ev\ (113\ kcal\ m^{-1}) \quad (1)$$

where hν is the photon energy

$$4H_2 + 4e^- \rightarrow 2H_2\ E^\circ_{red} = 0\ V \quad (2)$$

$$2H_2O \rightarrow 4H^+ + 4e^- + O_2\ E^\circ_{red} = 1.23V \quad (3)$$

6. Factors Affecting the Photochemical (PC) and Photoelectrochemical (PEC) Performance

The photochemical and photoelectrochemical (PEC) water-splitting performance primarily depends on the morphology, uniformity, and structural order of the nanomaterials used. In addition, the size and structure of the materials are also important factors in the PEC water-splitting mechanism. However, PEC water splitting differs from the photochemical process in that it involves an external bias, and the excitation and de-excitation of electrons occur at separate electrodes. Furthermore, a PEC system requires a three-electrode setup—comprising a working electrode, counter electrode, and a reference electrode—to complete the reaction. To achieve efficient water splitting using these processes, several factors must be considered, including the structure and morphology of the material, the bandgap and suitable band edge positions for water oxidation and reduction, as well as pH, pressure, and temperature. The basic phenomena involves in the PEC water splitting is shown in (Figure 3).

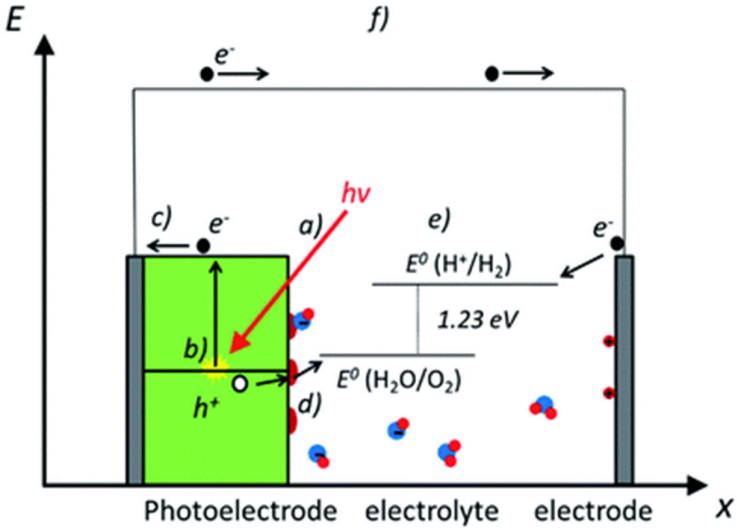

Figure 3. The scheme shows the basic phenomena involved in photoelectrochemical (PEC) water splitting: (a) interaction of mater with light, (b) generation of electron–hole pairs, (c) separation and transportation of charge (d), catalysis (e), water-splitting reaction (f), photocurrent associated with PEC water splitting [37]. Copyright 2020 Royal society of chemistry.

6.1. Crystalline Structure and Morphology

The structure and morphology of photocatalysts generally depend on the synthesis method and the specific steps involved; for instance, variations in crystal size, shape, and structure can result from changes in temperature and the use of different surfactants. In addition, morphology and dimensionality are strongly influenced by pH. The nucleation and growth behavior can be controlled by the concentration of OH^- ions [38]. The performance of crystalline materials compared to amorphous materials is typically superior. A well-known example is the enhanced photocurrent observed in annealed (crystalline) TiO_2 nanotubes compared to their amorphous counterparts. Figure 4 presents a comparison of the photodegradation performance of annealed and amorphous TiO_2, showing that amorphous TiO_2 can be transformed into crystalline TiO_2 at elevated temperatures around 300 °C. As a general rule, crystalline TiO_2 nanotubes demonstrate improved hydrogen production in PEC water splitting. Studies have shown that the crystallite size of TiO_2 nanotubes increases with increasing voltage during anodization. This is likely due to the fact that higher voltages favor the formation of larger crystal nuclei and enhanced crystallinity. In turn, this reduces the number of defect sites that promote electron–hole recombination, thus, significantly affecting photocurrent efficiency [34,39,40].

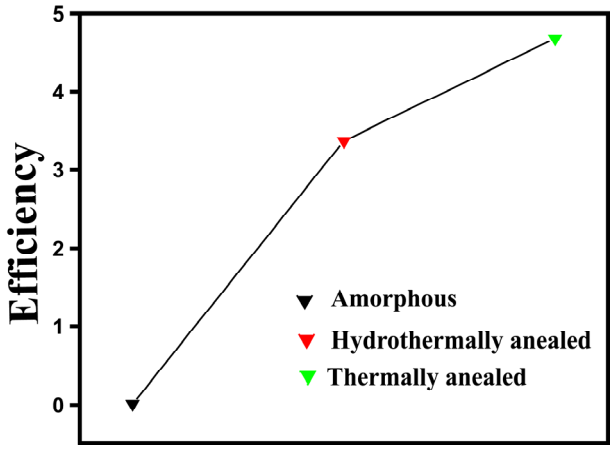

Figure 4. Photocurrent efficiency of different forms of TiO_2 nanotubes [40].

6.2. Bandgap

The electronic structure of semiconductors is typically described in terms of energy bands, which can be viewed as a range of energy resulting from the small energy differences between adjacent molecular orbitals [33]. For efficient PEC water splitting, bandgap energies in the range of 1.6 to 2.2 eV are essential. Semiconductors with large bandgaps are generally unable to absorb a significant portion of the visible light spectrum, resulting in reduced solar-to-hydrogen conversion efficiency [41]. The advantage of nanomaterials is their ability to modify bandgap energies to improve the PEC performance [42,43]. The bandgap can be reduced through the introduction of donor–acceptor species into the semiconductor. The band structure of various semiconductors in relation to the redox potential of water splitting is illustrated in Figure 5. Numerous strategies, including the modification of photocatalysts with transition metal cations, have been explored to improve solar energy utilization under visible light irradiation.

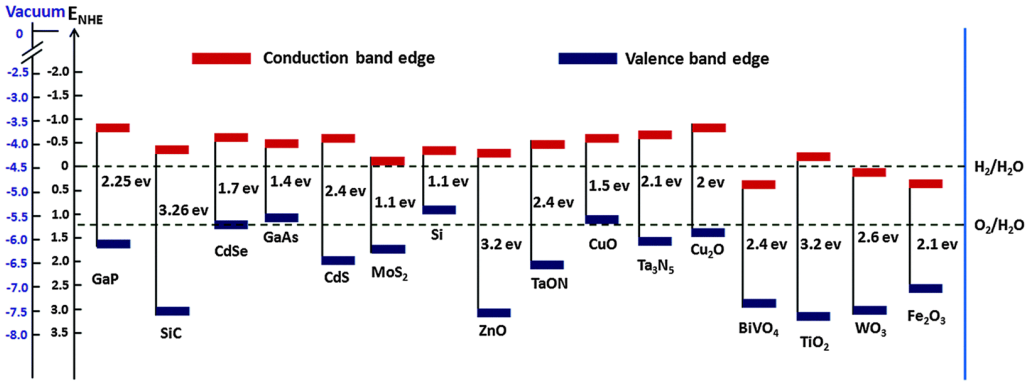

Figure 5. Schematic illustration of band position of various semiconductors vs. NHE and vacuum [44].

6.3. The Dependence on Temperature and Pressure

Temperature is an important parameter that plays a vital role in the performance of PEC cells. This is because catalytic activity, electrode kinetics, photoelectrode quantum efficiency, charge transfer, electrode stability, diffusion, and conductivity in the electrolyte, as well as ionic mobility, are all significantly influenced by temperature [45]. Typically, high temperatures are used in PEC experiments. However, improved PEC efficiency at low temperatures has also been reported. One study demonstrated a 95% increase in IPEC efficiency at 350 nm under low-temperature conditions [46]. Operating at low temperatures is particularly important, especially for fabricating PEC photoelectrodes from organic substrates with low melting points, and for studying interfacial physics to improve PEC performance. On the other hand, a study by Chong et al. [47] showed that temperatures above 80 °C can inhibit reactant adsorption, resulting in a reduced photocatalytic activity of TiO_2. These findings indicate that the optimal operational temperature varies depending on the material. Therefore, the temperature factor can be adjusted to enhance the photocatalytic activity. Additionally, enhancement of the bandgap with increasing pressure has also been reported [48].

6.4. Effect of pH

Experimental results have shown that the band edge potential can be altered by changes in the pH of the electrolyte solution [31]. Additionally, the pH of the solution influences the charge state of the metal oxides. A study by Nada et al. [49] demonstrated that an acidic medium favors greater hydrogen production than a basic medium. More broadly, PEC cells operate under a wide range of pH conditions. The pH of the electrolyte solution significantly affects the equilibrium of the reaction, which determines the net total charge as either positive, zero, or negative at the surface. However, in highly corrosive or extreme pH environments, minimizing photocorrosion is essential to maintain efficiency. The electrode surface deteriorates as the movement of ions takes place during the reaction. The stability of the photoelectrode in varying pH conditions can be improved by the incorporation of nanomaterials. Similarly, photocatalysts show enhanced performance and stability in the presence of buffered electrolyte solutions [50]. Other factors influencing PEC water splitting include the intensity of incident light, dopant-induced effects on grain nucleation, impurities, surface facet exposure, water adsorption/desorption kinetics related to pore structure, and preparation-dependent grain morphology.

6.5. Limitations of Photochemical vs. Photoelectrochemical Approaches

Photochemical and photoelectrochemical approaches both offer promising pathways for green hydrogen (H_2) production, each with their distinct advantages and limitations. Although the two processes differ fundamentally, the photochemical process operates with-

out the need for an external bias and can utilize suspended catalysts in solution, making it relatively simple, cost-effective, and attractive for large-scale applications. However, the photochemical approach suffers from low quantum efficiencies and poor charge separation, which result in significant electron–hole recombination [51]. In contrast, the photoelectrochemical process enhances charge separation through the application of an external bias or by employing photoelectrodes within a cell. This improves conversion efficiencies and provides better control over reaction kinetics. Ultimately, the choice between photochemical and photoelectrochemical approaches depends on the specific target application. The photochemical approach favors simplicity and low cost, while the photoelectrochemical method offers higher efficiency and tunability at the expense of increased system complexity.

7. Titanium Dioxide (TiO_2)

Over the years, TiO_2 has gained significant attention and has become one of the most extensively studied photocatalysts due to several advantages, such as low cost, high photocatalytic efficiency, non-toxicity, thermal and chemical stability, and a high refractive index [52]. However, its photocatalytic performance is hindered by the rapid recombination of photogenerated electron–hole pairs, backward reactions, and its wide bandgap (3.02–3.18 eV), which limits its activity in the visible region. The wide bandgap of pristine TiO_2 enables the absorption of only ultraviolet light ($\lambda \approx 380$ nm), which constitutes just 4–5% of the solar spectrum, thereby reducing solar-to-chemical conversion efficiency. Furthermore, the fast recombination of electron–hole pairs lowers the quantum efficiency [53]. To address this, various metal oxides and sulfides have been developed and employed in hydrogen evolution reactions. However, many of these materials exhibit limited stability under different pH conditions, which is critical during photocatalytic reactions. For example, sulfide-based photocatalysts degrade under solar irradiation due to the oxidation of sulfide ions to elemental sulfur [54]. Metal oxides such as $BiVO_4$, ZnO, WO_3, CuO, Fe_2O_3, and others generally suffer from rapid charge recombination and various stability issues. Fe_2O_3-based photocatalysts have short hole diffusion lengths, leading to quick charge recombination under solar irradiation. $BiVO_4$ is also prone to instability and fast charge recombination, and its band edge positions are suitable only for water oxidation [55–57]. Similarly, CuO is unstable due to rapid oxidation to Cu^{2+} and Cu^{1+} species [58].

On the other hand, TiO_2 is stable, inexpensive, suitable for water redox reactions, and abundantly available, making it one of the most promising candidates for water-splitting applications [33,59]. Among various TiO_2 nanomaterials, TiO_2 nanotubes have emerged as a particularly attractive option. However, the previously mentioned limitations of TiO_2 must be addressed to achieve higher efficiency. To overcome these challenges, numerous strategies have been developed. Notably, both metal and non-metal doping have been widely explored to enhance charge carrier separation and improve the optical absorption properties of TiO_2. Other techniques include the formation of heterojunctions to facilitate charge separation and transport, surface modification through the deposition of noble metals or inorganic acids, metal ion incorporation, and dye sensitization [60]. Alternatively, black TiO_2 nanoparticles have demonstrated superior photocatalytic activity compared to their pristine counterparts [61]. Additionally, TiO_2 nanowires have shown a better performance than nanorods, indicating that the morphology and size of TiO_2 nanostructures are critical factors influencing conversion efficiency [36,62]. Liu et al. [40] reported an enhancement in cell performance when using thermally annealed TiO_2 nanotubes, attributed to improved charge transport due to increased crystallinity. Scanning electron microscopy (SEM) cross-sectional images revealed that, prior to annealing, the nanotubes had smooth inner and outer wall morphology. Thermal annealing induced roughening of the inner tube

walls, while the diameter and outer wall remained largely unchanged. In contrast, water-annealed nanotubes showed pronounced morphological changes. The current–voltage (*I–V*) curves presented in the study indicated that water-annealed nanotubes exhibited approximately threefold higher dye adsorption compared to amorphous nanotubes. However, thermally annealed nanotubes achieved a superior solar cell performance, with a solar conversion efficiency of approximately η~4.65%.

Role of TiO_2 in HER

TiO_2 is a promising material for the hydrogen evolution reaction (HER) due to its unique electronic and physicochemical properties. Its wide bandgap provides strong oxidative stability and excellent resistance to photocorrosion, which is crucial for long-term operation in aqueous environments. However, the intrinsic HER activity of pristine TiO_2 is limited by its poor electrical conductivity and sluggish charge-transfer kinetics. These limitations can be effectively addressed through strategies such as metal or non-metal doping, defect engineering (e.g., introducing oxygen vacancies), and the formation of heterojunctions with conductive cocatalysts such as Pt, MoS_2, or graphene. These modifications introduce mid-gap states, enhance charge separation, and improve electron mobility. Importantly, the conduction band edge of TiO_2 lies at a sufficiently negative potential to thermodynamically favor proton reduction to H_2 under illumination, enabling efficient solar-driven HER. Furthermore, its tunable surface chemistry and high surface area in nanostructured forms provide abundant active sites and improve mass transport, making TiO_2 a highly versatile platform for the development of efficient and stable HER systems, particularly in photoelectrochemical cells.

8. TiO_2 Modification Strategies

8.1. Doping of Metal and Non-Metal

As a general rule, the functionality and efficiency of nanomaterials are significantly influenced by their lattice structure and surface composition. Literature reports indicate that modifying the crystal lattice of nanomaterials by introducing electronically active secondary species can markedly alter charge carrier dynamics and optical absorption properties. The deposition of certain metals facilitates the attraction of electrons to the metal particles deposited on TiO_2, thereby reducing electron–hole recombination and consequently enhancing photocatalytic activity [63]. The primary role of metallic dopants is to introduce additional energy levels within the bandgap, which shifts the optical absorption edge by lowering the energy barrier [64]. Among noble metals, Ag-modified TiO_2 is widely studied for hydrogen generation under low-energy UV illumination. Liu et al. [65] synthesized TiO_2 nanotubes decorated with Ag_2S nanoparticles, which were subsequently treated with acetonitrile and subjected to vacuum drying to obtain Ag_2S-decorated TiO_2 nanotubes with a narrower bandgap. Their results demonstrated a hydrogen production rate of 1.13 $mL/cm^2/h$, with excellent reproducibility. Similarly, Lalitha et al. [66] reported the impregnation of Ag^+ ions onto the TiO_2 surface, attributing the observed hydrogen evolution under solar irradiation to the interface formed by Ag ions on the TiO_2 surface layers. Among the various synthesis techniques, the sol–gel method is considered one of the simplest and most commonly used methods for nanoparticles synthesis. Its advantages include rapid processing, good compositional homogeneity, and operation at relatively low calcination temperatures and times, often resulting in nanoparticles with a high crystallinity and surface area [52].

Dholan et al. [67] employed a combination of room-temperature (RT) and sol–gel methods to synthesize Fe- and Cr-doped TiO_2. The photocatalytic performance of the doped TiO_2 was evaluated for H_2 production under visible light irradiation. The doped samples exhibited enhanced hydrogen evolution compared to undoped TiO_2, attributed to the role of Fe and Cr as electron trapping agents. In another study, Wu and Lee demonstrated that the photocatalytic H_2 generation from pure water and/or water containing sacrificial reagents significantly increased upon deposition of Pd, Ni, and Pt onto TiO_2. Additionally, enhanced hydrogen production using TiO_2 loaded with Cu metal in aqueous methanol solution has also been reported [68]. Zhu et al. [69] deposited Pt nanoparticles on hollow-sphere TiO_2 via a sol–gel technique for hydrogen generation. The inclusion of approximately 1.0 wt% Pt resulted in the highest H_2 evolution rate. This improvement was attributed to the surface dispersion of Pt nanoparticles, which effectively act as charge separators. Ismail et al. [63] reported the incorporation of PdO into a mesoporous TiO_2 network, leading to increased photocatalytic performance. They observed catalytic activity 4- and 2-times higher than that of commercial TiO_2-P_{25} and Pd/TiO_2-P_{25}, respectively. Huang et al. [70] applied a combined hydrothermal/sol–gel technique to synthesize co-doped TiO_2 nanorods with Rh and Nb. These nanorods were tested under visible and UV light irradiation for hydrogen production. Among the samples, $Ti_{0.996}Nb_{0.002}Rh_{0.002}O_2$ exhibited superior photocatalytic activity compared to pure TiO_2 and other co-doped materials. The enhanced performance was attributed to improved charge separation and the introduction of Rh, which creates impurity levels above the valence band of TiO_2.

Recent studies confirm that metal ion doping (cations) initiates a deep localization of d-states within the bandgap of TiO_2, thereby promoting charge carrier recombination. In contrast, anionic dopants are less prone to forming recombination centers and are generally more effective in enhancing photocatalytic activity [71]. Various anionic dopants, such as N, C, F, B, S, and Cl, have been extensively investigated for TiO_2 modification. Hou and co-workers [72] synthesized nitrogen (N)-doped TiO_2 nanotubes using a hydrothermal method. The resulting materials were immersed in deionized water and ammonia solutions of varying concentrations. Their findings showed that the sample treated with ammonia solution exhibited higher light absorption compared to that treated with water alone. They also observed that the morphology of TiO_2 was strongly influenced by the molar ratio between deionized water and ammonia solution. Moreover, nitrogen doping reduced the bandgap energy from 3.23 to 2.84 eV (Figure 6a), thereby significantly enhancing the visible-light activity of the N-doped TiO_2 nanotubes. More recently, McMananmon et al. [73] studied sulfur (S)-doped TiO_2 nanoparticles prepared via sol–gel synthesis. Their study revealed that sulfur atoms occupied interstitial sites within the TiO_2 crystal lattice, leading to the formation of surface states between the valence band (VB) and conduction band (CB). The bandgap energy was red-shifted from 3.2 to 1.7 eV, facilitating visible-light absorption as shown in Figure 6b. In 2004, Luo and co-workers [74] reported the synthesis of Br and Cl co-doped TiO_2 using a hydrothermal technique. Titanium chloride and hydrobromic acid served as sources of Ti and Br, respectively. The resulting material exhibited enhanced absorption in the visible region due to non-metal doping, which contributed to bandgap narrowing and improved solar-driven water-splitting efficiency.

In 2021, Khan et al. investigated the effects of both substitutional and interstitial nitrogen (N) doping on the bandgap of TiO_2. The researchers employed a straightforward nitridation method to synthesize N-doped TiO_2 nanotubes (NTs). N-doping in TiO_2 results in the formation of donor states below the conduction band and acceptor states above the valence band, which collectively contribute to a reduced bandgap and enhanced visible light absorption, as illustrated in Figure 7 [75].

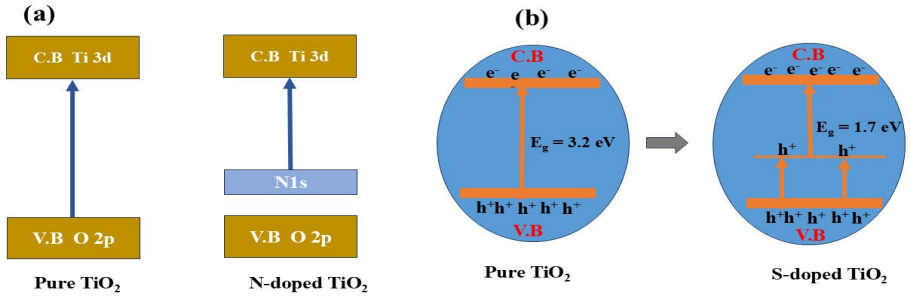

Figure 6. Schematic diagram of the energy band structure of pure TiO_2 and N-doped TiO_2 (**a**), and sulfur (S) doping narrowing the bandgap energy (**b**).

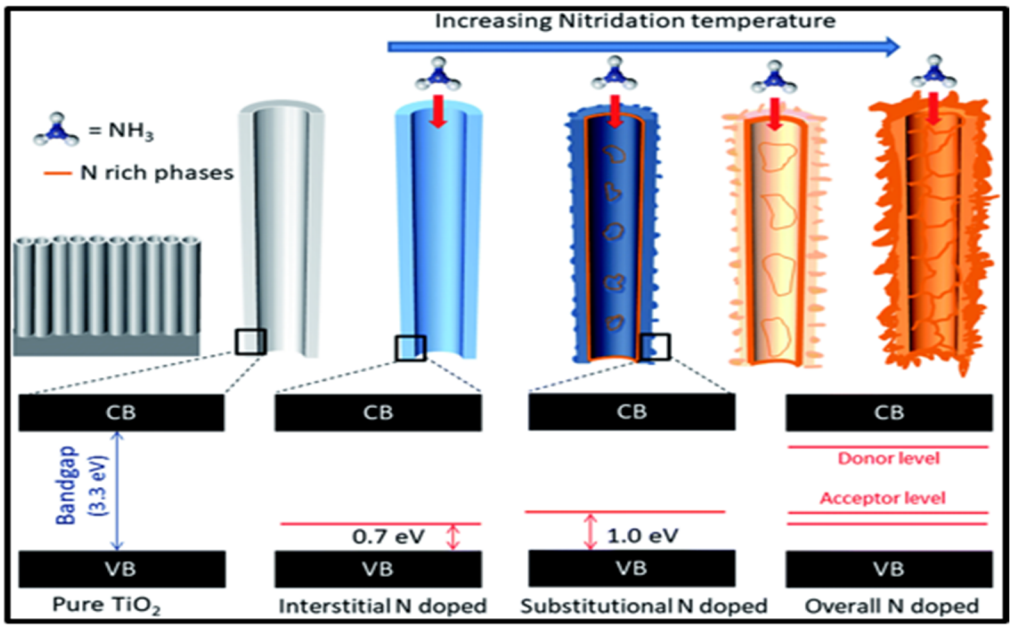

Figure 7. Schematic representation of N doping and the presence of interband states related to interstitial and substitutional doping. Adopted from Reference [75].

Recently, Fazil et al. synthesized copper (Cu)-doped TiO_2 nanoparticles (NPs) via hydrothermal synthesis. Doping levels of 1%, 2.5%, and 5% Cu were applied to TiO_2, resulting in a noticeable redshift in bandgap energies. Specifically, the bandgap of pure TiO_2 redshifted from 3.19 eV to 3.8 eV for the 2.5% Cu-doped sample. This shift was attributed to the formation of impurity states or vacancies between the valence band (VB) and conduction band (CB) induced by the dopants. Additionally, the authors hypothesized that a reduced bandgap could affect the photocatalyst's morphology, particle size, electronic, and optical properties [76]. Photoluminescence spectra, presented in Figure 8, demonstrated enhanced charge transfer and a reduced bandgap for the 2.5% Cu-doped TiO_2 NPs, leading to improved overall photochemical activity.

Most recently, Safinaz et al. synthesized pure TiO_2 loaded with metals (Co, Ni, and Rh) as cocatalysts using a hydrothermal synthesis procedure [77]. They observed a significant change in the bandgap energies upon loading these metallic cocatalysts. The bandgap of pure TiO_2 was found to be 2.97 eV, which redshifted to 2.6 eV after cocatalyst loading. The authors did not specify the exact cause of this bandgap reduction. However, they attributed the decrease to heterojunction formation between TiO_2 and the cocatalysts, which enhanced the photocatalytic performance. Although doping is widely used to tailor the properties of TiO_2, it also introduces several drawbacks. It can create defects such as vacancies and interstitials, which serve as charge recombination centers, thereby reducing photocatalytic

efficiency. Excessive doping may also impair crystallinity and induce undesirable phase transitions—for instance, promoting the anatase-to-rutile transformation. Moreover, improper doping can introduce deep impurity states within the bandgap, leading to charge trapping and recombination [78,79].

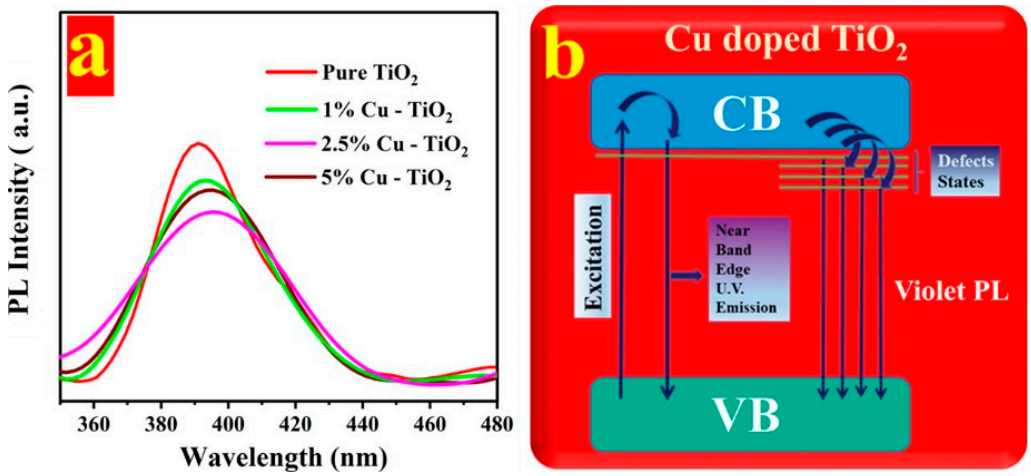

Figure 8. (**a**) PL spectra of Cu-doped TiO_2 and (**b**) scheme explaining the possible transitions. Adopted from reference [76].

8.2. Creation of Heterojunction

Global energy demand and the pursuit of environmentally friendly energy sources have been a critical issue in recent years. The transformation of solar energy into a storable energy medium is highly desirable [80]. While a single semiconductor can achieve direct water splitting, its effectiveness depends on two key criteria: appropriate redox potentials and strong absorption in the visible light region [81]. In general, suitable semiconductor photocatalysts must possess a wide bandgap with well-aligned valence band (VB) and conduction band (CB) positions, efficient separation of photoinduced charge carriers, high resistance to photocorrosion, and the ability to transfer energetic electrons. Although TiO_2 meets most of these requirements, its major limitation is that it can only absorb UV light, which constitutes approximately 4% of the solar spectrum [82]. A heterojunction is typically defined as the interface between two dissimilar semiconductors with mismatched band structures. Introducing heterojunctions—by coupling TiO_2 with other semiconductors or noble metals that have wider or narrower bandgaps—has been widely explored to overcome this limitation. The construction of such heterojunctions can significantly enhance light absorption, suppress the recombination of charge carriers, and produce a more stable photocatalyst [26]. Therefore, selecting a suitable cocatalyst is a critical and competitive step. A photocatalyst with a large surface area provides abundant active sites, and accurate band alignment is essential for efficient charge transfer between the two semiconductors [2,83]. Based on these considerations, heterojunctions are commonly classified into five types, as illustrated in Figure 9.

8.2.1. Type I Heterojunction

In a type-I heterojunction, the valence band (VB) of semiconductor 1 lies below and the conduction band (CB) of semiconductor 1 lies above those of semiconductor 2, as shown in Figure 9a. Therefore, under light illumination, both the photogenerated electrons and holes migrate from semiconductor 1 to semiconductor 2.

8.2.2. Type II Heterojunction

The type-II heterojunctions have a staggered band structure between the two applied semiconductors, which effectively inhibits the recombination of photoinduced electron–hole pairs. Semiconductors 1 and 2 possess distinct band potentials, as presented in Figure 9b. Upon light illumination, the transfer of a photogenerated hole in the type-II junction can easily take place from the valence band (VB) of semiconductor 2 to the VB of semiconductor 1, provided that the VB of semiconductor 2 is lower than that of semiconductor 1. Conversely, if the conduction band (CB) of semiconductor 1 is higher than the CB of semiconductor 2, the transfer of electrons from semiconductor 1 to semiconductor 2 takes place, causing the spatial separation of charge carriers. This leads to an increase in the electron lifetime and reduces electron–hole recombination. Furthermore, when sufficient energy is supplied to excite semiconductor 1, semiconductor 2 acts as an electron–hole acceptor. Notably, the construction of type-II heterojunctions is highly promising for photocatalytic applications. Hence, the type-II heterojunction is considered one of the best heterojunction-based photocatalysts, according to the literature [84–88].

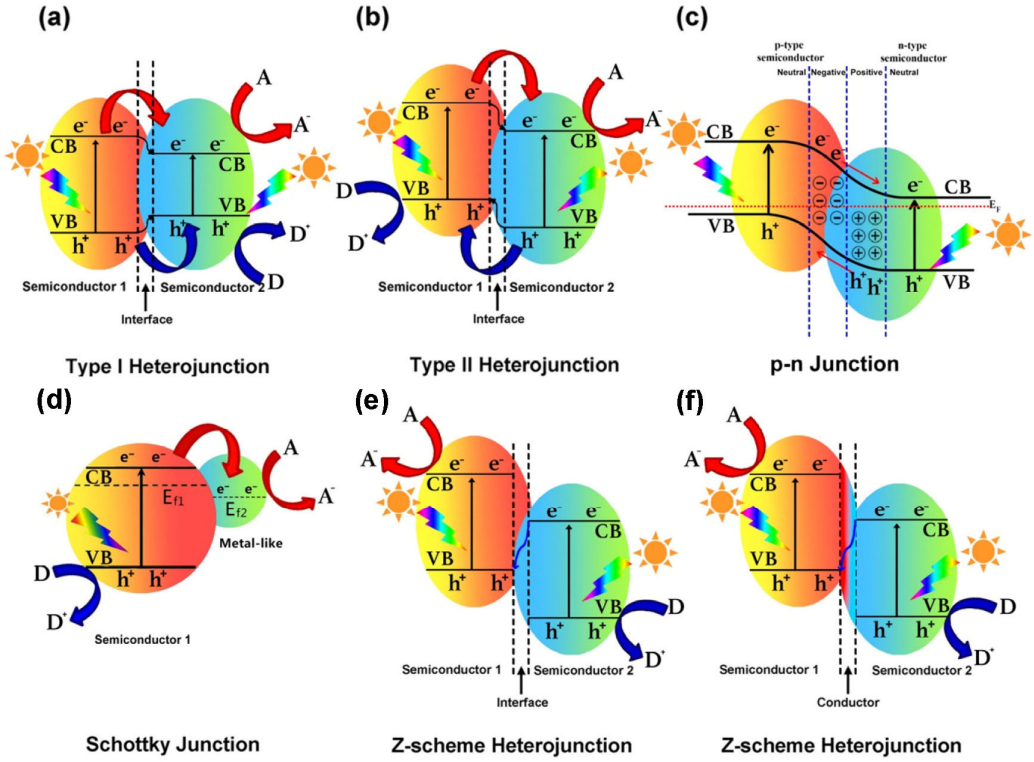

Figure 9. Various types of heterojunctions and their respective band structure: (**a**) type-I hetero junction, (**b**) type-II heterojunction, (**c**) p-n junction or heterojunction, (**d**) Schottky junction, (**e**) and (**f**) Z-scheme junctions. A, D, and E_F denote electron accepter, electron donor, and Fermi level, respectively [89]. Copyright 2019 Elsevier Ltd.

8.2.3. p-n Heterojunction

The improvement of electron–hole pair separation in other heterojunction types is often insufficient to effectively suppress electron–hole recombination in semiconductors. In this context, the idea of assembling a p-n heterojunction is presented to boost photocatalytic performance by providing a built-in electric field to speed up charge carrier transfer. The p-n heterojunction exhibits higher charge separation efficiency than the type-II heterojunction, thereby enhancing photocatalytic activity. The p-n heterojunction is obtained by combining p-type and n-type semiconductor materials [90–95]. As the Fermi level varies depending on the semiconductor type, the Fermi level of the p-type semiconductor is located closer

to the valence band (VB), while that of the n-type is closer to the conduction band (CB). Therefore, electron–hole diffusion occurs between the semiconductors even before light illumination. As soon as the Fermi level reach equilibrium, the circulation of charge carriers stabilizes [96]. The creation of a built-in electric field due to different Fermi-level positions in semiconductors is responsible for the separation of electron–hole pairs, as shown in Figure 9c.

Zha et al. [97] demonstrated the photocatalytic performance of a TiO_2/ZnO nanocomposite under UV light for methyl orange degradation. Their results showed an excellent photocatalytic activity (97% in 30 min), attributed to its large surface area and hierarchical structure. The SEM and TEM images (Figure 10A, Figure 10B, and Figure 10C, respectively) of the as-prepared heterojunction reveal a multi-layered, fan-bladed structure with an average length ranging between 2.5 and 3 μm. Figure 10D presents the HRTEM image, where the planes (101) and (100) correspond to TiO_2 and ZnO, respectively. Figure 10E shows the photocatalytic mechanism of the TiO_2/ZnO heterojunction. The ZnO energy bandgap (3.37 eV) is slightly greater than that of TiO_2, thus presenting a more negative conduction band (CB) and valence band (VB) potentials. Upon UV illumination, photons excite electrons from the VB to the CB in both semiconductors. Due to the conduction band offset, electrons preferentially migrate to the CB of TiO_2. Meanwhile, holes thermodynamically transfer from the VB of TiO_2 to the VB of ZnO, enhancing the photocatalytic activity.

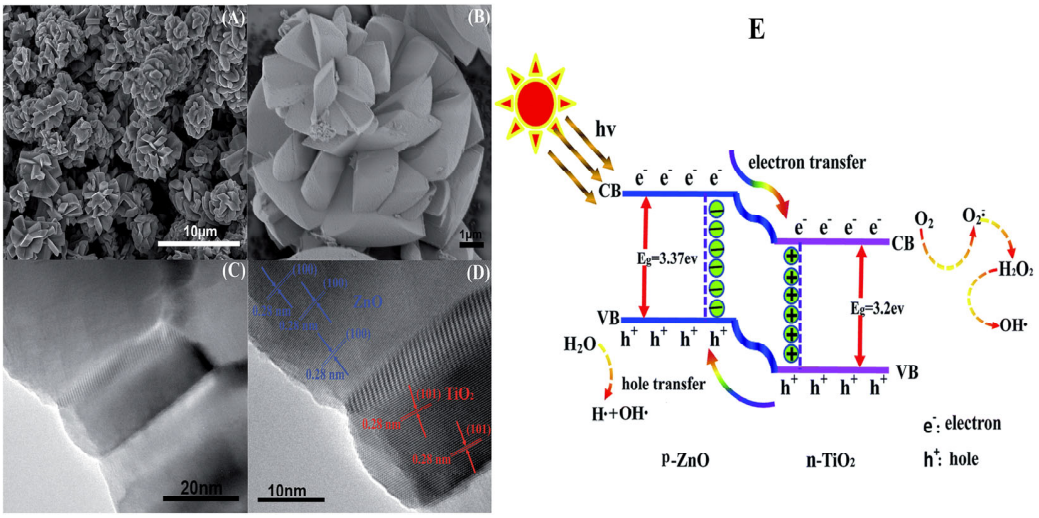

Figure 10. SEM, TEM, and HRTEM images of fan blades (**A**–**D**), respectively. Schematic diagram illustration of p-n heterojunction (**E**) [97]. Copyright 2015, Royal Society of Chemistry (RCS).

Guo et al. [98] reported the successful synthesis of $SrTiO_3$/TiO_2 nanosheets using a hydrothermal process, which resulted in a porous structure and a high surface area. An enhancement in charge carrier separation was observed under UV light irradiation. The photoinduced charge transfer and separation in the $SrTiO_3$/TiO_2 composite are illustrated in Figure 11.

In another study, Liu et al. [99] constructed a CuS/TiO_2 heterojunction using solvothermal synthesis, exhibiting a spherical, cake-like shape. The resulting material exhibited suppressed charge recombination and efficient charge transfer, attributed to the well-established built-in electric field formed at the CuS/TiO_2 p-n heterojunction. In addition, the heterojunction enhanced light absorption due to a narrowed bandgap, thereby improving photocatalytic activity. The charge-transfer mechanism in CuS/TiO_2 is shown in Figure 12.

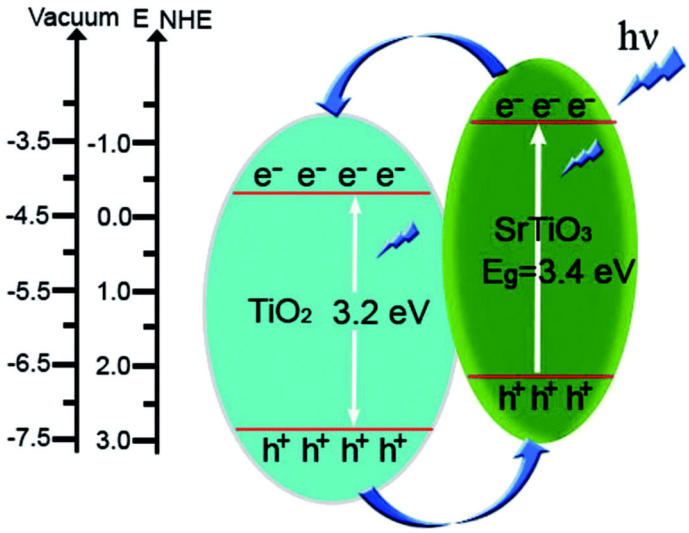

Figure 11. Scheme showing the bandgap energy and charge transfer or separation pathways in $SrTiO_3/TiO_2$ composite [98]. Copyright 2015, Royal Society of Chemistry (RSC).

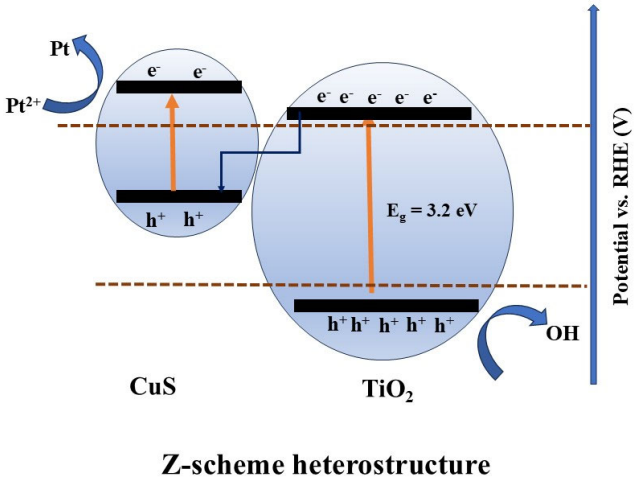

Figure 12. Scheme representing the charge transfer in CuS/TiO_2.

Recently, Dongxiang et al. [100] carried out density functional theory (DFT) and nonadiabatic molecular dynamics (NAMD) analysis on a TiO_2-based heterojunction. In this study, they formed a heterojunction between anatase TiO_2 (A-TiO_2) and rutile TiO_2 (R-TiO_2). The study suggested that the A-TiO_2/R-TiO_2 heterojunction effectively prolongs the lifetime of photogenerated electron–hole pairs and improves the redox capability. Furthermore, the A-TiO_2/R-TiO_2 heterojunction demonstrates a higher solar-to-hydrogen (STH) efficiency under varying pH conditions.

8.2.4. Schottky Junction

The heterojunction between a semiconductor and a metal-like material is called a Schottky junction, which is highly effective at generating a space–charge separation region. Due to its favorable interfacial structure, electrons rapidly transfer from one component to the other, facilitating Fermi level alignment and significantly hindering charge recombination, thereby improving photocatalytic performance [89]. Copper (Cu), cobalt (Co), and nickel (Ni) are considered potential candidates in photocatalysis because of their high work function. Combining these cocatalysts with TiO_2 can form a Schottky junction at the interface, resulting in a built-in electric field, or can create active sites, both of which en-

hance electron–hole separation and thereby improve the photocatalytic activity of pristine TiO_2 [101].

Qiu et al. [102] constructed a Cu/TiO_2 Schottky junction using the solvothermal synthesis procedure. They used different percentages of Cu with TiO_2, with optimal charge separation observed for the 10% Cu–TiO_2 junction. The enhancement in charge separation was attributed to the formation of the built-in electric field. This built-in electric field further facilitates charge separation, thereby enhancing photocatalytic hydrogen production.

Recently, Medrano et al. [103] modified commercial TiO_2 with mono- and bimetallic (Au, Pd, and AuPd) nanoparticles using the chemical reduction method. This study reported that Au, Pd, and AuPd, in combination with TiO_2, form a Schottky barrier that enhances electron–hole separation and photocatalytic H_2 production. The Schottky junction is formed by the high-work-function metals Au, Pd, and AuPd with TiO_2, which creates an internal electric field. This internal field facilitates effective charge separation and inhibits electron–hole recombination, thereby enhancing photocatalytic activity. The schematic diagram for the AuPd-loaded TiO_2 is shown in Figure 13, illustrating the photocatalytic mechanism under UV and visible light irradiation.

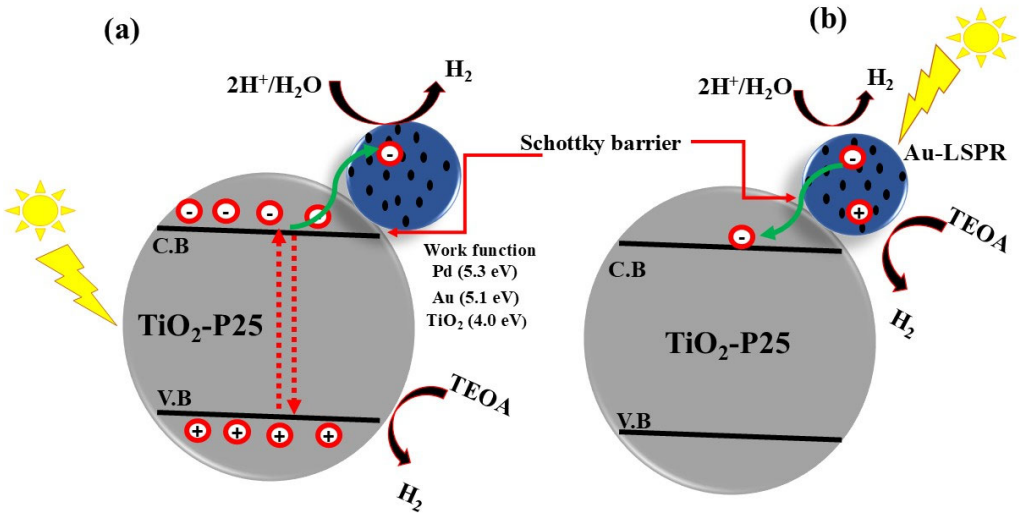

Figure 13. Scheme representing photocatalytic mechanism under (**a**) UV, and (**b**) visible light irradiation. The corresponding work function and Schottky barrier formation of the Au, Pd, and TiO_2 are also given. Adopted from references.

8.2.5. Z-Scheme Heterojunction

All the earlier-mentioned heterojunctions can effectively increase charge separation in photocatalysts. However, the redox capacity of the semiconductor composite materials is often compromised, since the reduction and oxidation reactions typically occur on the semiconductor with the less favorable redox potentials [104]. In 1979, Brad et al. [105] reported the Z-scheme photocatalytic method for the first time to suppress the above-mentioned issue. Inspired by the natural photosynthesis process in plants, the Z-scheme enables both effective photogenerated charge carrier separation and the preservation of strong redox capability.

However, limited application of the Z-scheme system using a redox mediator in the liquid phase has been noted [106]. The development of an all-solid-state photocatalytic Z-scheme heterojunction system is highly desirable [107], which leads to the proposal of a solid conductive material that acts as an electron mediator—or even operates in the absence of a mediator (Figure 9e,f). Nanoscale metals possess excellent electrical conductivity, which makes them ideal candidates as electron mediators in the construction of Z-scheme systems [108–110]. In contrast, Yu et al. [111] in 2013 advanced the concept of a

mediator-free Z-scheme heterojunction. In the direct Z-scheme charge-transfer mechanism, photogenerated electrons transfer from the conduction band (CB) of semiconductor 2 to the valence band (VB) of semiconductor 1, where they recombine with the photogenerated holes. Unlike the traditional liquid-phase Z-scheme, the all-solid-state Z-scheme system can be widely applied in both gas–solid and liquid–solid photocatalytic systems [107].

As mentioned above, constructing an indirect Z-scheme by introducing an electron mediator between the two semiconductors can enhance charge transfer. In contrast, a direct Z-scheme system improves photocatalytic activity by enabling a tight interface between the two components [112–115]. In this context, Li et al. [116] reported a direct Z-scheme photocatalyst composed of g-C_3N_4 nanosheets (g-C_3N_4 NS) and $CuInS_2$ (denoted as GsC). Their results showed that GsC exhibited a significantly higher photocurrent density compared to neat $CuInS_2$ and g-C_3N_4 NS, as illustrated in Figure 14a, indicating efficient charge separation. Figure 14b further confirms the lowest charge-transfer resistance (R_{et}) of GsC across all light intensities when compared to bare $CuInS_2$ and g-C_3N_4 NS, suggesting easier electron migration in GsC toward the electrolyte protons, facilitating H_2 generation. Remarkably, the photoluminescence (PL) lifetime of GsC showed a 6-fold enhancement, as clearly depicted in Figure 14c, demonstrating superior performance in separating photogenerated electron–hole pairs (Figure 14d).

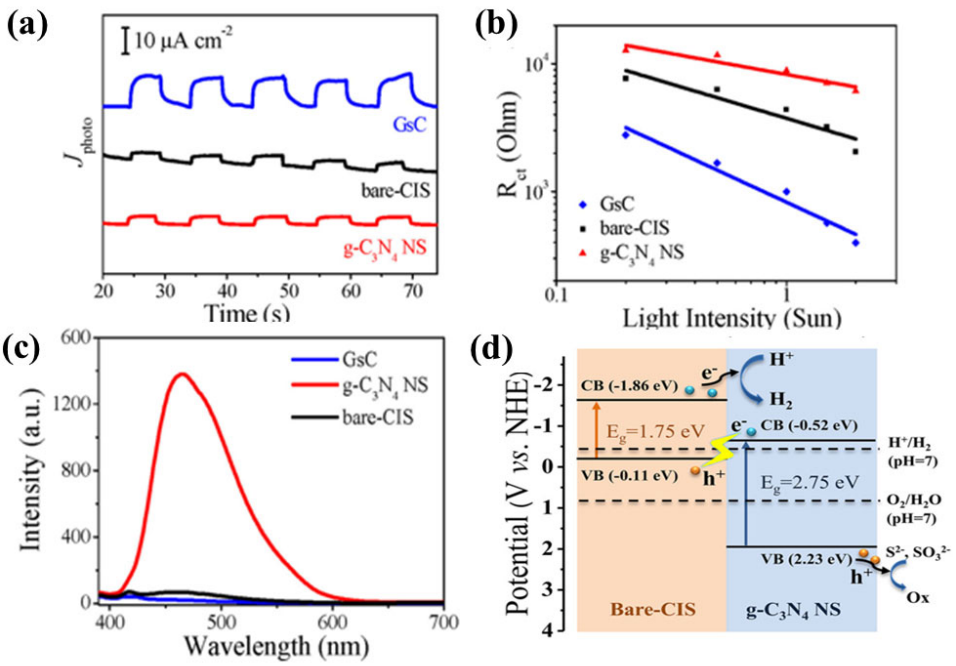

Figure 14. Transient photocurrent of the samples at λ > 420 nm (**a**), the effect of the light intensities on the R_{et} (**b**), PL spectra of the samples (**c**), band potential of the materials used for designing a Z-scheme system (**d**) [116]. Copyright 2018 American Chemical Society.

In 2021, Lv et al. [117] established a mesoporous Cu_2O/TiO_2 Z-scheme system for photocatalytic hydrogen evolution using the solvothermal synthesis method. The study suggested that the combination of TiO_2 with Cu_2O improved both stability and charge carrier mobility. Moreover, the Cu_2O/TiO_2 composite enhances the number of active sites, which are crucial for the rapid migration of hydrogen ions (H^+) and the generation of hydrogen gas (H_2). The Cu_2O/TiO_2 Z-scheme system retains the strong reduction potential of the conduction band (CB) of Cu_2O and the oxidation potential of the valence band (VB) of TiO_2, resulting in improved photocatalytic performance.

Recently, Liu et al. [99] constructed a CuS/TiO_2 Z-scheme heterojunction via the co-precipitation synthesis method. The study reported that Z-scheme construction using CuS

and TiO_2 improves charge transfer due to the difference in carrier concentrations between the two semiconductors. Electrons diffuse from TiO_2 to CuS, while holes move from CuS to TiO_2. This bidirectional charge diffusion between the semiconductors leads to the formation of a built-in electric field, which is the primary driving force for enhanced charge separation and transport to oxidation and reduction sites, thereby improving photocatalytic activity.

It is clear from the above discussion that Z-scheme and type-II heterojunctions are comparable in terms of energy band structure but follow different charge-transfer mechanisms. In this regard, how to differentiate between the two types of heterojunctions has become a hot topic in scientific studies. The presence of a mediator in the heterojunction indicates a Z-scheme system in a hybrid photocatalyst. However, in the absence of a mediator, the possibility of both type-II and Z-scheme mechanisms exists. Therefore, more accurate strategies are required to investigate the charge-transfer mechanism. Ohno et al. [118] used dual-beam photoacoustic (DB-PA) spectroscopy to confirm the Z-scheme pathway in the WO_3/g-C_3N_4 system, in comparison to a type-II heterojunction. In addition, the detection of reactive oxygen species such as superoxide (O_2^-) and hydroxyl (•OH) radicals relative to redox potentials using chemical probe techniques can also be proposed as a strategy to verify the Z-scheme mechanism.

The TiO_2 heterojunction with other metal oxides is widely employed to enhance photocatalytic performance. However, it has several shortcomings. Poor band alignment and interfacial defects can promote electron–hole recombination instead of facilitating efficient charge separation. Many materials are used to form heterojunctions (for example, CdS, MoS_2) with TiO_2, but they often suffer from photochemical instability, leading to performance degradation over time [119]. Moreover, the fabrication of high-quality, defect-free heterojunctions is complex and difficult to scale for industrial applications. Furthermore, lattice mismatches and environmental concerns regarding certain materials, such as toxic heavy metals, pose additional challenges to the practical deployment of TiO_2-based heterojunctions.

8.3. Inorganic Acid Modification of TiO_2

The use of inorganic acids as surface modifiers for TiO_2 photocatalysts can significantly alter their surface charge carrier properties in neutral water. The addition of new surface groups to TiO_2 can greatly facilitate the separation of photogenerated electron–hole pairs, thereby improving photocatalytic activity. As a general rule, surface modification with inorganic acids enhances O_2 adsorption on the photocatalyst surface, leading to superior photocatalytic performance [120]. Cui et al. [121] reported the surface modification of TiO_2 with phosphate. The results showed better photocatalytic activity for phosphate-modified TiO_2 than for unmodified TiO_2. They proposed that phosphate modification does not affect the crystal phase composition, optical properties, or crystallinity. Hence, the enhancement in O_2 adsorption is primarily related to the linkage of phosphate groups on the TiO_2 surface. Phosphate-modified TiO_2 alters the surface terminal groups from –Ti–OH to –Ti–O–P–OH groups [122]. In fact, the –Ti–O–P–OH group is more acidic than the –Ti–OH group, as the dissociation of –Ti–O–P–OH in water occurs to some extent, producing –Ti–O–P–O^- and hydrogen ions (H^+). Thus, increased surface acidity is expected to favor O_2 adsorption. This interpretation is supported by the temperature-programmed desorption of ammonia (NH_3-TPD) curves for treated and untreated TiO_2, and further corroborated by FT-IR spectra of adsorbed pyridine. Additionally, Cui et al. [121] modified TiO_2 with various inorganic acids, including nitric acid, sulfuric acid, and phosphoric acid. After thermal treatment at 500 °C, HNO_3 was removed from the modified TiO_2 due to its instability, whereas H_3PO_4 and H_2SO_4 remained as residues on the TiO_2 surface. Generally, the greater the amount of chemically adsorbed O_2, the stronger the surface photovoltage spectroscopy (SPS) intensities. The

SPS intensities followed the order of TiO_2 < TiO_2/HNO_3 < TiO_2/H_2SO_4 < TiO_2/H_3PO_4, confirming that TiO_2 treated with H_2SO_4 and H_3PO_4 had a larger amount of chemically adsorbed O_2. The photocatalytic activity of TiO_2 treated with H_3PO_4 and H_2SO_4 was clearly higher than that of the untreated samples. These experimental results indicate that TiO_2 surface modification is a key strategy for enhancing its photocatalytic activity.

8.4. Modification of TiO_2 by Creating Oxygen Vacancies

A scientifically important and interesting type of TiO_2 modification involves the creation of oxygen vacancies by removing oxygen atoms. Reduced TiO_2 is generally represented as TiO_{2-x}, where x denotes the estimated density of oxygen vacancies. The Magnéli phase, a titanium suboxide with the general formula Ti_nO_{2n-1}, is formed by removing a small percentage of oxygen and has attracted significant attention due to its potential to enhance the photocatalytic activity of TiO_2. Magnéli-phase titanium suboxide was first produced in the 1950s using hydrogenation [71]. The photocatalytic hydrogen evolution performance of metal- and non-metal-doped TiO_2, as well as heterojunctions (e.g., Z-scheme, S-scheme, etc.) involving TiO_2 and other semiconductors, is summarized in Table 1. The hydrogen evolution rates are listed in a dedicated column, while the reaction parameters are provided separately. Moreover, to enable a better comparison of the photochemical and photoelectrochemical performance of TiO_2-based photocatalysts, the photocurrent densities of TiO_2-based photoelectrodes are also included in Table 2.

Table 1. Photocatalytic (photochemical) hydrogen evolution for TiO_2 doped with metals and non-metals, and making it a heterojunction with other semiconductors under different reaction conditions.

Entry	Catalysts	H_2 Production	Parameters	Ref
1	Co, Ni, and Cu-doped TiO_2	85 μmol h^{-1}	UV irradiation Methanol	[123]
2	Ga or Ni co-doped TiO_2	35 μmol h^{-1}	125 W Hg lamp ≥ 400 nm Methanol	[124]
3	Cu and S-TiO_2	7.5 mmol g^{-1} h^{-1}	500 W Xe lamp, using quartz reactor	[125]
4	Ni-doped TiO_2	180 μmol h^{-1}	300 W Hg lamp methanol	[126]
5	Bi-doped TiO_2	4500 μmol g^{-1} h^{-1}	500 W, using Xe lamp	[127]
6	N-doped TiO_2	102 μmol g^{-1} h^{-1}	Visible light irradiations	[128]
7	B-N-TiO_2	85 μmol/50 mg methanol	36 W light lamp	[129]
8	S-doped TiO_2	164 mmol g^{-1} h^{-1}	Visible light (1.5 G) irradiation ≥ 400 nm	[130]
9	Nb-doped TiO_2	0.7 mmol g^{-1} h^{-1}	Hg(UV)-Xe (Vis) lamp (500 W)	[131]
10	TiO_2-SiO_2	1.7 cm^3/h.gcat	300 W Xe lamp, visible light irradiation (λ > 420 nm)	[132]
11	Cu_3P/TiO_2 Z-scheme	607 μmol g^{-1} h^{-1}	300 W Xe lamp Water, methanol	[133]
12	$ZnIn_2S_4$/ TiO_2 Z-scheme	6.5 mmol g^{-1} h^{-1}	300 W Xe lamp irradiation TEOA	[134]
13	NiO-TiO_2 p-n heterojunction	228 μmol g^{-1} h^{-1}	300 W Xe lamp AM 1.5 G filter Water, methanol	[135]
14	Ru-doped TiO_2	23.9 mmol g^{-1} h^{-1}	UV-LED lamp, methanol	[77]
15	g-C_3N_4/ TiO_2 S-scheme	134 μmol g^{-1} h^{-1}	300 W Xe lamp TEOA	[136]

Table 2. Photoelectrochemical (PEC) performance of different TiO_2-based heterojunctions.

Entry	Photoelectrode	Photocurrent Density	Parameters	References
1	Pure TiO_2 and N-TiO_2	180 μA/cm_2	<0.3 V vs. Ag/AgCl, AM 1.5 G, 1 Sun illumination, and 1 M KOH	[75]
2	TiO_2-$BiFeO_3$/rGO	1.7 mA/cm^2	0.6 V vs. Ag/AgCl, AM 1.5 G, 1 Sun illumination, 0.1 M NaOH	[100]
3	TiO_2/$BiVO_4$	2.2 mA/cm^2	at 1.23 Vs RHE, 1 Sun illumination, AM 1.5 G	[137]
4	BiVO4/TiO2 NFs	1.7 mA/cm^2	at 1.23 V vs. RHE, AM 1.5 G illumination, 1 M Na_2SO_3	[138]
5	R-TiO_2@$BiVO_4$	2.1 mA/cm^2	0.45 V vs. RHE, AM 1.5G illumination.	[139]
6	TiO_2@CoNi-LDHs	4.4 mA/cm^2	1.23 V vs. RHE, AM 1.5 G illumination, 1 M Na_2SO_3, pH 6.8	[140]
7	TiO_2%40CoNi-LDHsTiO_2@c/$FeTiO_3$	6.03 mA/cm^2	1.5 V vs. SCE	[141]
8	ZnS/CdS/TiO_2	7.45 mA/cm^2	0.25 M S/1 M Na_2S	[142]
9	TiO_2 NPs	100.12 μA cm^{-2}	1.23 V vs. RHE, 0.5 M Na_2SO_4, 1.5 G illumination	[143]

9. Conclusions and Future Direction

In summary, TiO_2-based photocatalysts and their application in the production of green energy (H_2) have been discussed. Strategies such as doping, heterojunction formation, acidic modification, oxygen vacancy engineering, and the influence of temperature and pressure have been discussed to improve charge separation. Metal and non-metal doping in TiO_2 reduces the bandgap and improves charge separation by enhancing visible light absorption. Likewise, forming a heterojunction between TiO_2 and another semiconductor improves charge separation by forming a built-in electric field at the interface. Acidic modification favors enhanced hydrogen production compared to basic media because it modifies the band edge potential. Temperature and pressure also affect the photocatalytic activity of TiO_2. For instance, temperatures above 80 °C can hinder reactant adsorption, while increased pressure can widen the bandgap, thereby suppressing the photocatalytic activity of TiO_2. In addition, a comparative table has been constructed to summarize the photocatalytic hydrogen production performance of pure TiO_2 and its combinations with other semiconductors, metals, and non-metals. To conclude, heterojunction formation and doping are the most promising and effective strategies for enhancing charge separation and transfer efficiency in TiO_2 by engineering the bandgap and creating a built-in electric field.

This review provides critical insights into bandgap tuning, charge carrier dynamics, and morphology-dependent effects, which offer practical guidance for the rational design of next-generation TiO_2-based photocatalysts. Furthermore, it highlights the synergistic effects of combining multiple modification strategies, helping to overcome challenges in optimizing TiO_2 for scalable and sustainable hydrogen production.

Finally, considering the inherent limitations of TiO_2, future research should focus on developing new catalysts with improved performance via scalable and cost-effective synthesis routes. The synthesis process should strategically incorporate metallic dopants to effectively engineer the bandgap, thereby enhancing light absorption and charge separation. This should be complemented by the controlled deposition of cocatalysts to further boost catalytic activity and stability. Additionally, advancements in in situ characterization techniques and computational modeling will play a pivotal role in optimizing charge dynamics and defect engineering at the atomic level. The integration of these strategies is

expected to accelerate the development of highly efficient and durable systems, ultimately enabling the practical implementation of solar-driven hydrogen production technologies.

Author Contributions: Conceptualization, M.N.; methodology, M.N. and N.K.; validation, M.I.Q., and Z.S.; writing—original draft preparation, M.N.; writing—review and editing, N.K. and M.I.Q.; visualization, M.I.Q. and Z.S.; supervision, M.N.; project administration, M.N.; funding acquisition, M.N. All authors have read and agreed to the published version of the manuscript.

Funding: This research was funded by the National Research and Development Agency of Chile (ANID) under the FONDECYT Project N° 11251269.

Acknowledgments: The authors thank the National Research and Development Agency of Chile (ANID) for financial support through Project FONDECYT N° 11251269.

Conflicts of Interest: The authors declare that there are no conflicts of interest.

References

1. Lewis, N.S. Developing a scalable artificial photosynthesis technology through nanomaterials by design. *Nat. Nanotechnol.* **2016**, *11*, 1010–1019. [CrossRef] [PubMed]
2. Moniz, S.J.A.; Shevlin, S.A.; Martin, D.J.; Guo, Z.-X.; Tang, J. Visible-light driven heterojunction photocatalysts for water splitting—A critical review. *Energy Environ. Sci.* **2015**, *8*, 731–759. [CrossRef]
3. Lubitz, W.; Tumas, W. Hydrogen: An Overview. *Chem. Rev.* **2007**, *107*, 3900–3903. [CrossRef]
4. *2020 World Population Data Sheet*; Population Reference Bureau: Washington, DC, USA, 2020; p. 4.
5. Reddy, C.V.; Reddy, K.R.; Shetti, N.P.; Shim, J.; Aminabhavi, T.M.; Dionysiou, D.D. Hetero-nanostructured metal oxide-based hybrid photocatalysts for enhanced photoelectrochemical water splitting—A review. *Int. J. Hydrogen Energy* **2020**, *45*, 18331–18347. [CrossRef]
6. Nisar, M.; Bernard, F.L.; Duarte, E.; Chaban, V.; Einloft, S. New polysulfone microcapsules containing metal oxides and ([BMIM][NTf2]) ionic liquid for CO_2 capture. *J. Environ. Chem. Eng.* **2021**, *9*, 104781. [CrossRef]
7. Nisar, M.; Thue, P.S.; Maghous, M.B.; Geshev, J.; Lima, E.C.; Einloft, S. Polysulfone metal-activated carbon magnetic nanocomposites with enhanced CO_2capture. *RSC Adv.* **2020**, *10*, 34595–34604. [CrossRef]
8. Lewis, E.; Chamel, O.; Mohsenin, M.; Ots, E.; White, E.T. Intergovernmental Panel on Climate Change. In *Sustainaspeak*, 1st ed.; Routledge: New York, NY, USA, 2018; pp. 153–154. [CrossRef]
9. Cai, J.; Shen, J.; Zhang, X.; Ng, Y.H.; Huang, J.; Guo, W.; Lin, C.; Lai, Y. Light-Driven Sustainable Hydrogen Production Utilizing TiO_2 Nanostructures: A Review. *Small Methods* **2018**, *3*, 1800184. [CrossRef]
10. Xiao, L.; Wu, S.-Y.; Li, Y.-R. Advances in solar hydrogen production via two-step water-splitting thermochemical cycles based on metal redox reactions. *Renew. Energy* **2012**, *41*, 1–12. [CrossRef]
11. Cook, T.R.; Dogutan, D.K.; Reece, S.Y.; Surendranath, Y.; Teets, T.S.; Nocera, D.G. Solar Energy Supply and Storage for the Legacy and Nonlegacy Worlds. *Chem. Rev.* **2010**, *110*, 6474–6502. [CrossRef]
12. Nocera, D.G. The Artificial Leaf. *Acc. Chem. Res.* **2012**, *45*, 767–776. [CrossRef]
13. Wang, M.; Han, K.; Zhang, S.; Sun, L. Integration of organometallic complexes with semiconductors and other nanomaterials for photocatalytic H2 production. *Co-ord. Chem. Rev.* **2015**, *287*, 1–14. [CrossRef]
14. Steinfeld, A. Solar thermochemical production of hydrogen—A review. *Sol. Energy* **2005**, *78*, 603–615. [CrossRef]
15. Graf, D.; Monnerie, N.; Roeb, M.; Schmitz, M.; Sattler, C. Economic comparison of solar hydrogen generation by means of thermochemical cycles and electrolysis. *Int. J. Hydrogen Energy* **2008**, *33*, 4511–4519. [CrossRef]
16. Van Gerven, T.; Mul, G.; Moulijn, J.; Stankiewicz, A. A review of intensification of photocatalytic processes. *Chem. Eng. Process. Process. Intensif.* **2007**, *46*, 781–789. [CrossRef]
17. Balayeva, N.O. Mamiyev, Chapter 5—Integrated processes involving adsorption, photolysis, and photocatalysis. In *Hybrid and Combined Processes for Air Pollution Control: Methodologies, Mechanisms and Effect of Key Parameters*; Assadi, A., Amrane, A., Nguyen, T.A., Eds.; Elsevier: Amsterdam, The Netherlands, 2022; pp. 117–153. [CrossRef]
18. Maeda, K.; Domen, K. Solid Solution of GaN and ZnO as a Stable Photocatalyst for Overall Water Splitting under Visible Light. *Chem. Mater.* **2010**, *22*, 612–623. [CrossRef]
19. Fujishima, A.; Honda, K. Electrochemical Photolysis of Water at a Semiconductor Electrode. *Nature* **1972**, *238*, 37–38. [CrossRef]
20. Wang, Y.; Suzuki, H.; Xie, J.; Tomita, O.; Martin, D.J.; Higashi, M.; Kong, D.; Abe, R.; Tang, J. Mimicking Natural Photosynthesis: Solar to Renewable H_2 Fuel Synthesis by Z-Scheme Water Splitting Systems. *Chem. Rev.* **2018**, *118*, 5201–5241. [CrossRef]
21. Kudo, A.; Miseki, Y. Heterogeneous photocatalyst materials for water splitting. *Chem. Soc. Rev.* **2009**, *38*, 253–278. [CrossRef]

22. Yang, H.; Chen, F.; Wang, X.; Qian, J.; Wang, J.; Li, J.; Lv, C.; Li, L.; Bandaru, S.; Gao, J. Self-Reconstructed Spinel with Enhanced SO_4^{2-} Adsorption and Highly Exposed Co^{3+} From Heterostructure Boosts Activity and Stability at High Current Density for Overall Water Splitting. *Adv. Funct. Mater.* **2025**, *35*, 2419978. [CrossRef]
23. Wang, J.-L.; Wang, C.; Lin, W. Metal–Organic Frameworks for Light Harvesting and Photocatalysis. *ACS Catal.* **2012**, *2*, 2630–2640. [CrossRef]
24. Kataoka, Y.; Sato, K.; Miyazaki, Y.; Masuda, K.; Tanaka, H.; Naito, S.; Mori, W. Photocatalytic hydrogen production from water using porous material [Ru2(p-BDC)2]n. *Energy Environ. Sci.* **2009**, *2*, 397–400. [CrossRef]
25. Wang, C.; Xie, Z.; Dekrafft, K.E.; Lin, W. Doping Metal–Organic Frameworks for Water Oxidation, Carbon Dioxide Reduction, and Organic Photocatalysis. *J. Am. Chem. Soc.* **2011**, *133*, 13445–13454. [CrossRef]
26. Maeda, K. Z-Scheme Water Splitting Using Two Different Semiconductor Photocatalysts. *ACS Catal.* **2013**, *3*, 1486–1503. [CrossRef]
27. Abe, R. Recent progress on photocatalytic and photoelectrochemical water splitting under visible light irradiation. *J. Photochem. Photobiol. C Photochem. Rev.* **2010**, *11*, 179–209. [CrossRef]
28. Li, R.; Zhang, F.; Wang, D.; Yang, J.; Li, M.; Zhu, J.; Zhou, X.; Han, H.; Li, C. Spatial separation of photogenerated electrons and holes among {010} and {110} crystal facets of BiVO. *Nat. Commun.* **2013**, *4*, 1432. [CrossRef]
29. Yang, J.; Wang, D.; Han, H.; Li, C. Roles of Cocatalysts in Photocatalysis and Photoelectrocatalysis. *Acc. Chem. Res.* **2013**, *46*, 1900–1909. [CrossRef]
30. Liao, C.-H.; Huang, C.-W.; Wu, J.C.S. Hydrogen Production from Semiconductor-based Photocatalysis via Water Splitting. *Catalysts* **2012**, *2*, 490–516. [CrossRef]
31. Jiang, D.; Zhao, H.; Jia, Z.; Cao, J.; John, R. Photoelectrochemical behaviour of methanol oxidation at nanoporous TiO_2 film electrodes. *J. Photochem. Photobiol. A Chem.* **2001**, *144*, 197–204. [CrossRef]
32. Zhang, P.; Zhang, J.; Gong, J. Tantalum-based semiconductors for solar water splitting. *Chem. Soc. Rev.* **2014**, *43*, 4395–4422. [CrossRef]
33. Ahmad, H.; Kamarudin, S.; Minggu, L.; Kassim, M. Hydrogen from photo-catalytic water splitting process: A review. *Renew. Sustain. Energy Rev.* **2015**, *43*, 599–610. [CrossRef]
34. Josny, J.; Jinu, M.; Soney, C.G. Nanomaterials for photoelectrochemical water splitting—Review. *Int. J. Hydrogen Energy* **2018**, *43*, 4804–4817. [CrossRef]
35. Wilke, T.; Schricker, D.; Rolf, J.; Kleinermanns, K. Solar Water Splitting by Semiconductor Nanocomposites and Hydrogen Storage with Quinoid Systems. *Open J. Phys. Chem.* **2012**, *2*, 195–203. [CrossRef]
36. Wolcott, A.; Smith, W.A.; Kuykendall, T.R.; Zhao, Y.; Zhang, J.Z. Photoelectrochemical Water Splitting Using Dense and Aligned TiO_2 Nanorod Arrays. *Small* **2009**, *5*, 104–111. [CrossRef]
37. Ros, C.; Andreu, T.; Morante, J.R. Photoelectrochemical water splitting: A road from stable metal oxides to protected thin film solar cells. *J. Mater. Chem. A* **2020**, *8*, 10625–10669. [CrossRef]
38. Meshram, S.; Adhyapak, P.; Mulik, U.; Amalnerkar, D. Facile synthesis of CuO nanomorphs and their morphology dependent sunlight driven photocatalytic properties. *Chem. Eng. J.* **2012**, *204–206*, 158–168. [CrossRef]
39. Zhang, Z.; Wang, P. Optimization of photoelectrochemical water splitting performance on hierarchical TiO_2 nanotube arrays. *Energy Environ. Sci.* **2012**, *5*, 6506–6512. [CrossRef]
40. Liu, N.; Albu, S.P.; Lee, K.; So, S.; Schmuki, P. Water annealing and other low temperature treatments of anodic TiO_2 nanotubes: A comparison of properties and efficiencies in dye sensitized solar cells and for water splitting. *Electrochim. Acta* **2012**, *82*, 98–102. [CrossRef]
41. Yin, W.-J.; Tang, H.; Wei, S.-H.; Al-Jassim, M.M.; Turner, J.; Yan, Y. Band structure engineering of semiconductors for enhanced photoelectrochemical water splitting: The case ofTiO. *Phys. Rev. B Condens. Matter Mater Phys* **2010**, *82*. [CrossRef]
42. Wang, J.; Sun, H.; Huang, J.; Li, Q.; Yang, J. Band Structure Tuning of TiO_2 for Enhanced Photoelectrochemical Water Splitting. *J. Phys. Chem. C* **2014**, *118*, 7451–7457. [CrossRef]
43. Vishwakarma, A.K.; Tripathi, P.; Srivastava, A.; Sinha, A.; Srivastava, O. Band gap engineering of Gd and Co doped BiFeO3 and their application in hydrogen production through photoelectrochemical route. *Int. J. Hydrogen Energy* **2017**, *42*, 22677–22686. [CrossRef]
44. Tamirat, A.G.; Rick, J.; Dubale, A.A.; Su, W.-N.; Hwang, B.-J. Using hematite for photoelectrochemical water splitting: A review of current progress and challenges. *Nanoscale Horiz.* **2016**, *1*, 243–267. [CrossRef] [PubMed]
45. Dias, P.; Lopes, T.; Andrade, L.; Mendes, A. Temperature effect on water splitting using a Si-doped hematite photoanode. *J. Power Sources* **2014**, *272*, 567–580. [CrossRef]
46. Nie, Q.; Yang, L.; Cao, C.; Zeng, Y.; Wang, G.; Wang, C.; Lin, S. Interface optimization of ZnO nanorod/CdS quantum dots heterostructure by a facile two-step low-temperature thermal treatment for improved photoelectrochemical water splitting. *Chem. Eng. J.* **2017**, *325*, 151–159. [CrossRef]
47. Chong, M.N.; Jin, B.; Chow, C.W.K.; Saint, C. Recent developments in photocatalytic water treatment technology: A review. *Water Res.* **2010**, *44*, 2997–3027. [CrossRef]

48. Al-Agel, F.A.; Suleiman, J.; Khan, S.A. Studies on silicon quantum dots prepared at different working pressure. *Results Phys.* **2017**, *7*, 1128–1134. [CrossRef]
49. Nada, A.; Hamed, H.; Barakat, M.; Mohamed, N.; Veziroglu, T. Enhancement of photocatalytic hydrogen production rate using photosensitized TiO_2/RuO_2-MV^{2+}. *Int. J. Hydrogen Energy* **2008**, *33*, 3264–3269. [CrossRef]
50. Fekete, M.; Riedel, W.; Patti, A.F.; Spiccia, L. Photoelectrochemical water oxidation by screen printed ZnO nanoparticle films: Effect of pH on catalytic activity and stability. *Nanoscale* **2014**, *6*, 7585–7593. [CrossRef]
51. Yanagi, R.; Zhao, T.; Solanki, D.; Pan, Z.; Hu, S. Charge Separation in Photocatalysts: Mechanisms, Physical Parameters, and Design Principles. *ACS Energy Lett.* **2022**, *7*, 432–452. [CrossRef]
52. Ismael, M. A review and recent advances in solar-to-hydrogen energy conversion based on photocatalytic water splitting over doped-TiO_2 nanoparticles. *Sol. Energy* **2020**, *211*, 522–546. [CrossRef]
53. Gong, J.; Zhang, Y.; Yue, T.; Lu, Y. Improving built-in electric fields for effective photocatalytic activity in the rationally designed electron transfer pathway of TiO_2@MoS_2/Bi_2S. *J. Mater. Chem. A* **2024**, *12*, 10838–10851. [CrossRef]
54. Mamiyev, Z.; Balayeva, N.O. Metal Sulfide Photocatalysts for Hydrogen Generation: A Review of Recent Advances. *Catalysts* **2022**, *12*, 1316. [CrossRef]
55. Khan, N.; Stelo, F.; Santos, G.H.; Rossi, L.M.; Gonçalves, R.V.; Wender, H. Recent advances on Z-scheme engineered $BiVO_4$-based semiconductor photocatalysts for CO_2 reduction: A review. *Appl. Surf. Sci. Adv.* **2022**, *11*, 100289. [CrossRef]
56. Khan, N.; Koche, A.; Khan, W.; Nogueira, P.A.; Jamil, A.; Pieper, Y.; Toma, F.M.; Nascimento, O.R.; Gonçalves, R.V.; Khan, S. Optimizing Photocatalytic Water Oxidation by FeMnOx Bimetallic Cocatalyst on Zn-Doped $BiVO_4$ via Magnetron Sputter Deposition. *Appl. Catal. A Gen.* **2025**, *704*, 120389. [CrossRef]
57. Khan, N.; Koche, A.; Centurion, H.A.; Rabelo, L.; Bettini, J.; dos Santos, G.T.; Souza, F.L.; Gonçalves, R.V.; Khan, S. Triggering Synergy between p-Type Sputter-Deposited FeMnOx or FeNiOx and W-Doped $BiVO_4$ for Enhanced Oxygen Evolution. *ACS Appl. Energy Mater.* **2024**, *7*, 2129–2141. [CrossRef]
58. Ali, S.; Razzaq, A.; Kim, H.; In, S.-I. Activity, selectivity, and stability of earth-abundant CuO/Cu2O/Cu^0-based photocatalysts toward CO_2 reduction. *Chem. Eng. J.* **2022**, *429*. [CrossRef]
59. Balayeva, N.O.; Mamiyev, Z.; Dillert, R.; Zheng, N.; Bahnemann, D.W. Rh/TiO_2-Photocatalyzed Acceptorless Dehydrogenation of N-Heterocycles upon Visible-Light Illumination. *ACS Catal.* **2020**, *10*, 5542–5553. [CrossRef]
60. Dhakshinamoorthy, A.; Navalon, S.; Corma, A.; Garcia, H. Photocatalytic CO_2 reduction by TiO_2 and related titanium containing solids. *Energy Environ. Sci.* **2012**, *5*, 9217–9233. [CrossRef]
61. Isimjan, T.T.; Rohani, S.; Ray, A.K. Photoelectrochemical water splitting for hydrogen generation on highly ordered TiO_2 nanotubes fabricated by using Ti as cathode. *Int. J. Hydrogen Energy* **2012**, *37*, 103–108. [CrossRef]
62. Chen, H.M.; Chen, C.K.; Liu, R.-S.; Zhang, L.; Zhang, J.; Wilkinson, D.P. Nano-architecture and material designs for water splitting photoelectrodes. *Chem. Soc. Rev.* **2012**, *41*, 5654–5671. [CrossRef]
63. Ismail, A.A. Mesoporous PdO–TiO_2 nanocomposites with enhanced photocatalytic activity. *Appl. Catal. B. Environ.* **2012**, *117–118*, 67–72. [CrossRef]
64. Babu, V.J.; Vempati, S.; Uyar, T.; Ramakrishna, S. Review of one-dimensional and two-dimensional nanostructured materials for hydrogen generation. *Phys. Chem. Chem. Phys.* **2015**, *17*, 2960–2986. [CrossRef]
65. Liu, X.; Liu, Z.; Lu, J.; Wu, X.; Chu, W. Silver sulfide nanoparticles sensitized titanium dioxide nanotube arrays synthesized by in situ sulfurization for photocatalytic hydrogen production. *J. Colloid Interface Sci.* **2014**, *413*, 17–23. [CrossRef]
66. Lalitha, K.; Reddy, J.K.; Sharma, M.V.P.; Kumari, V.D.; Subrahmanyam, M. Continuous hydrogen production activity over finely dispersed Ag_2O/TiO_2 catalysts from methanol:water mixtures under solar irradiation: A structure–activity correlation. *Int. J. Hydrogen Energy* **2010**, *35*, 3991–4001. [CrossRef]
67. Dholam, R.; Patel, N.; Adami, M.; Miotello, A. Hydrogen production by photocatalytic water-splitting using Cr- or Fe-doped TiO_2 composite thin films photocatalyst. *Int. J. Hydrogen Energy* **2009**, *34*, 5337–5346. [CrossRef]
68. Wu, N.-L.; Lee, M.-S. Enhanced TiO_2 photocatalysis by Cu in hydrogen production from aqueous methanol solution. *Int. J. Hydrogen Energy* **2004**, *29*, 1601–1605. [CrossRef]
69. Zhu, Z.; Kao, C.-T.; Tang, B.-H.; Chang, W.-C.; Wu, R.-J. Efficient hydrogen production by photocatalytic water-splitting using Pt-doped TiO_2 hollow spheres under visible light. *Ceram. Int.* **2016**, *42*, 6749–6754. [CrossRef]
70. Huang, J.; Li, G.; Zhou, Z.; Jiang, Y.; Hu, Q.; Xue, C.; Guo, W. Efficient photocatalytic hydrogen production over Rh and Nb codoped TiO2 nanorods. *Chem. Eng. J.* **2018**, *337*, 282–289. [CrossRef]
71. Rahimi, N.; Pax, R.A.; Gray, E.M. Review of functional titanium oxides. I: TiO_2 and its modifications. *Prog. Solid State Chem.* **2016**, *44*, 86–105. [CrossRef]
72. Hou, X.; Wang, C.-W.; Zhu, W.-D.; Wang, X.-Q.; Li, Y.; Wang, J.; Chen, J.-B.; Gan, T.; Hu, H.-Y.; Zhou, F. Preparation of nitrogen-doped anatase TiO2 nanoworm/nanotube hierarchical structures and its photocatalytic effect. *Solid State Sci.* **2014**, *29*, 27–33. [CrossRef]

73. McManamon, C.; O'Connell, J.; Delaney, P.; Rasappa, S.; Holmes, J.D.; Morris, M.A. A facile route to synthesis of S-doped TiO_2 nanoparticles for photocatalytic activity. *J. Mol. Catal. A Chem.* **2015**, *406*, 51–57. [CrossRef]
74. Luo, H.; Takata, T.; Lee, Y.; Zhao, J.; Domen, K.; Yan, Y. Photocatalytic Activity Enhancing for Titanium Dioxide by Co-doping with Bromine and Chlorine. *Chem. Mater.* **2004**, *16*, 846–849. [CrossRef]
75. Khan, S.; Ruwer, T.L.; Khan, N.; Köche, A.; Lodge, R.W.; Coelho-Júnior, H.; Sommer, R.L.; Santos, M.J.L.; Malfatti, C.F.; Bergmann, C.P.; et al. Revealing the true impact of interstitial and substitutional nitrogen doping in TiO_2 on photoelectrochemical applications. *J. Mater. Chem. A* **2021**, *9*, 12214–12224. [CrossRef]
76. Fazil, M.; Alshehri, S.M.; Mao, Y.; Ahmad, T. Enhanced Photo/Electrocatalytic Hydrogen Evolution by Hydrothermally Derived Cu-Doped TiO_2 Solid Solution Nanostructures. *Langmuir* **2024**, *40*, 4063–4076. [CrossRef]
77. Thabet, S.M.; Abdelhamid, H.N.; Ibrahim, S.A.; El-Bery, H.M. Boosting photocatalytic water splitting of TiO2 using metal (Ru, Co, or Ni) co-catalysts for hydrogen generation. *Sci. Rep.* **2024**, *14*, 1–10. [CrossRef]
78. Gomes, J.; Lincho, J.; Domingues, E.; Quinta-Ferreira, R.M.; Martins, R.C. N–TiO_2 Photocatalysts: A Review of Their Characteristics and Capacity for Emerging Contaminants Removal. *Water* **2019**, *11*, 373. [CrossRef]
79. Mani, S.S.; Rajendran, S.; Mathew, T.; Gopinath, C.S. A review on the recent advances in the design and structure–activity relationship of TiO_2-based photocatalysts for solar hydrogen production. *Energy Adv.* **2024**, *3*, 1472–1504. [CrossRef]
80. Resasco, J.; Zhang, H.; Kornienko, N.; Becknell, N.; Lee, H.; Guo, J.; Briseno, A.L.; Yang, P. TiO_2/$BiVO_4$ Nanowire Heterostructure Photoanodes Based on Type II Band Alignment. *ACS Cent. Sci.* **2016**, *2*, 80–88. [CrossRef]
81. Raziq, F.; Qu, Y.; Zhang, X.; Humayun, M.; Wu, J.; Zada, A.; Yu, H.; Sun, X.; Jing, L. Enhanced Cocatalyst-Free Visible-Light Activities for Photocatalytic Fuel Production of g-C_3N_4 by Trapping Holes and Transferring Electrons. *J. Phys. Chem. C* **2015**, *120*, 98–107. [CrossRef]
82. Ghasemi, S.; Esfandiar, A.; Setayesh, S.R.; Habibi-Yangjeh, A.; Gholami, M.R. Synthesis and characterization of TiO_2–graphene nanocomposites modified with noble metals as a photocatalyst for degradation of pollutants. *Appl. Catal. A Gen.* **2013**, *462–463*, 82–90. [CrossRef]
83. Humayun, M.; Raziq, F.; Khan, A.; Luo, W. Modification strategies of TiO_2 for potential applications in photocatalysis: A critical review. *Green Chem. Lett. Rev.* **2018**, *11*, 86–102. [CrossRef]
84. Kim, W.J.; Jang, E.; Park, T.J. Enhanced visible-light photocatalytic activity of ZnS/g-C_3N_4 type-II heterojunction nanocomposites synthesized with atomic layer deposition. *Appl. Surf. Sci.* **2017**, *419*, 159–164. [CrossRef]
85. Wang, H.; Yuan, X.; Wang, H.; Chen, X.; Wu, Z.; Jiang, L.; Xiong, W.; Zeng, G. Facile synthesis of Sb_2S_3/ultrathin g-C_3N_4 sheets heterostructures embedded with g-C3N4 quantum dots with enhanced NIR-light photocatalytic performance. *Appl. Catal. B Environ.* **2016**, *193*, 36–46. [CrossRef]
86. Jiang, D.; Li, J.; Xing, C.; Zhang, Z.; Meng, S.; Chen, M. Two-Dimensional $CaIn_2S_4$/g-C_3N_4 Heterojunction Nanocomposite with Enhanced Visible-Light Photocatalytic Activities: Interfacial Engineering and Mechanism Insight. *ACS Appl. Mater. Interfaces* **2015**, *7*, 19234–19242. [CrossRef]
87. Chen, W.; Liu, T.-Y.; Huang, T.; Liu, X.-H.; Yang, X.-J. Novel mesoporous P-doped graphitic carbon nitride nanosheets coupled with $ZnIn_2S_4$nanosheets as efficient visible light driven heterostructures with remarkably enhanced photo-reduction activity. *Nanoscale* **2016**, *8*, 3711–3719. [CrossRef]
88. Chen, W.; Hua, Y.-X.; Wang, Y.; Huang, T.; Liu, T.-Y.; Liu, X.-H. Two-dimensional mesoporous g-C_3N_4 nanosheet-supported $MgIn_2S_4$ nanoplates as visible-light-active heterostructures for enhanced photocatalytic activity. *J. Catal.* **2017**, *349*, 8–18. [CrossRef]
89. Ren, Y.; Zeng, D.; Ong, W.-J. Interfacial engineering of graphitic carbon nitride (g-C_3N_4)-based metal sulfide heterojunction photocatalysts for energy conversion: A review. *Chin. J. Catal.* **2019**, *40*, 289–319. [CrossRef]
90. Guo, F.; Shi, W.; Wang, H.; Han, M.; Li, H.; Huang, H.; Liu, Y.; Kang, Z. Facile fabrication of a CoO/g-C_3N_4p–n heterojunction with enhanced photocatalytic activity and stability for tetracycline degradation under visible light. *Catal. Sci. Technol.* **2017**, *7*, 3325–3331. [CrossRef]
91. Chu, J.; Han, X.; Yu, Z.; Du, Y.; Song, B.; Xu, P. Highly Efficient Visible-Light-Driven Photocatalytic Hydrogen Production on CdS/Cu_7S_4/g-C_3N_4 Ternary Heterostructures. *ACS Appl. Mater. Interfaces* **2018**, *10*, 20404–20411. [CrossRef]
92. Liu, G.; Zhao, G.; Zhou, W.; Liu, Y.; Pang, H.; Zhang, H.; Hao, D.; Meng, X.; Li, P.; Kako, T.; et al. In Situ Bond Modulation of Graphitic Carbon Nitride to Construct p–n Homojunctions for Enhanced Photocatalytic Hydrogen Production. *Adv. Funct. Mater.* **2016**, *26*, 6822–6829. [CrossRef]
93. Jiang, D.; Chen, L.; Zhu, J.; Chen, M.; Shi, W.; Xie, J. Novel p–n heterojunction photocatalyst constructed by porous graphite-like C_3N_4 and nanostructured BiOI: Facile synthesis and enhanced photocatalytic activity. *Dalton Trans.* **2013**, *42*, 15726–15734. [CrossRef]
94. Dong, F.; Zhao, Z.; Xiong, T.; Ni, Z.; Zhang, W.; Sun, Y.; Ho, W.K. In situ construction of g-C_3N_4/g-C_3N_4 metal-free heterojunction for enhanced visible-light photocatalysis. *ACS Appl. Mater. Interfaces* **2013**, *5*, 11392–11401. [CrossRef]

95. Qin, Z.; Wang, M.; Li, R.; Chen, Y. Novel Cu_3P/g-C_3N_4 p-n heterojunction photocatalysts for solar hydrogen generation. *Sci. China Mater.* **2018**, *61*, 861–868. [CrossRef]
96. Putri, L.K.; Ng, B.-J.; Ong, W.-J.; Lee, H.W.; Chang, W.S.; Chai, S.-P. Engineering nanoscale p–n junction: Via the synergetic dual-doping of p-type boron-doped graphene hybridized with n-type oxygen-doped carbon nitride for enhanced photocatalytic hydrogen evolution. *J. Mater. Chem. A* **2018**, *6*, 3181–3194. [CrossRef]
97. Zha, R.; Nadimicherla, R.; Guo, X. Ultraviolet photocatalytic degradation of methyl orange by nanostructured TiO_2/ZnO heterojunctions. *J. Mater. Chem. A* **2015**, *3*, 6565–6574. [CrossRef]
98. Guo, E.; Yin, L. Tailored $SrTiO_3$/TiO_2 heterostructures for dye-sensitized solar cells with enhanced photoelectric conversion performance. *J. Mater. Chem. A* **2015**, *3*, 13390–13401. [CrossRef]
99. Liu, J.; Sun, X.; Fan, Y.; Yu, Y.; Li, Q.; Zhou, J.; Gu, H.; Shi, K.; Jiang, B. P-N Heterojunction Embedded CuS/TiO_2 Bifunctional Photocatalyst for Synchronous Hydrogen Production and Benzylamine Conversion. *Small* **2024**, *20*, e2306344. [CrossRef]
100. Li, D.; Li, R.; Zhou, D.; Qin, X.; Yan, W. The formation of S-scheme anatase/rutile TiO_2 heterojunction and the enhancement of solar-to-hydrogen efficiency driven by dual electric field synergy. *Fuel* **2025**, *388*. [CrossRef]
101. Hong, J.W.; Wi, D.H.; Lee, S.-U.; Han, S.W. Metal–Semiconductor Heteronanocrystals with Desired Configurations for Plasmonic Photocatalysis. *J. Am. Chem. Soc.* **2016**, *138*, 15766–15773. [CrossRef]
102. Qiu, P.; Zhang, Y.; Cheng, G. Precursor self-derived Cu@TiO2 hybrid Schottky junction for enhanced solar-to-hydrogen evolution. *Int. J. Hydrogen Energy* **2022**, *47*, 10628–10637. [CrossRef]
103. Méndez-Medrano, A.A.; Bahena-Uribe, D.; Dragoe, D.; Clavaguéra, C.; Colbeau-Justin, C.; Báez, J.P.P.; Rodríguez-López, J.L.; Remita, H. Enhanced Photocatalytic Activity of Surface-Modified TiO_2 with Bimetallic AuPd Nanoalloys for Hydrogen Generation. *Sol. RRL* **2024**, *8*. [CrossRef]
104. Qi, K.; Cheng, B.; Yu, J.; Ho, W. A review on TiO_2-based Z-scheme photocatalysts. *Chin. J. Catal.* **2017**, *38*, 1936–1955. [CrossRef]
105. Bard, A.J.; Fox, M.A. Artificial Photosynthesis: Solar Splitting of Water to Hydrogen and Oxygen. *Acc. Chem. Res.* **1995**, *28*, 141–145. [CrossRef]
106. Li, H.; Tu, W.; Zhou, Y.; Zou, Z. Z-Scheme Photocatalytic Systems for Promoting Photocatalytic Performance: Recent Progress and Future Challenges. *Adv. Sci.* **2016**, *3*, 1500389. [CrossRef] [PubMed]
107. Zhou, P.; Yu, J.; Jaroniec, M. All-Solid-State Z-Scheme Photocatalytic Systems. *Adv. Mater.* **2014**, *26*, 4920–4935. [CrossRef]
108. Wang, M.; Han, Q.; Li, L.; Tang, L.; Li, H.; Zhou, Y.; Zou, Z. Construction of an all-solid-state artificial Z-scheme system consisting of Bi_2WO_6/Au/CdS nanostructure for photocatalytic CO_2 reduction into renewable hydrocarbon fuel. *Nanotechnology* **2017**, *28*, 274002. [CrossRef] [PubMed]
109. Zhang, N.; Xie, S.; Weng, B.; Xu, Y.-J. Vertically aligned ZnO–Au@CdS core–shell nanorod arrays as an all-solid-state vectorial Z-scheme system for photocatalytic application. *J. Mater. Chem. A* **2016**, *4*, 18804–18814. [CrossRef]
110. Zhao, W.; Xie, L.; Zhang, M.; Ai, Z.; Xi, H.; Li, Y.; Shi, Q.; Chen, J. Enhanced photocatalytic activity of all-solid-state g-C_3N_4 /Au/P25 Z-scheme system for visible-light-driven H2 evolution. *Int. J. Hydrogen Energy* **2016**, *41*, 6277–6287. [CrossRef]
111. Yu, J.; Wang, S.; Low, J.; Xiao, W. Enhanced photocatalytic performance of direct Z-scheme g-C3N4–TiO2 photocatalysts for the decomposition of formaldehyde in air. *Phys. Chem. Chem. Phys.* **2013**, *15*, 16883–16890. [CrossRef]
112. Xu, Q.; Zhang, L.; Yu, J.; Wageh, S.; Al-Ghamdi, A.A.; Jaroniec, M. Direct Z-scheme photocatalysts: Principles, synthesis, and applications. *Mater. Today* **2018**, *21*, 1042–1063. [CrossRef]
113. Wang, S.; Zhu, B.; Liu, M.; Zhang, L.; Yu, J.; Zhou, M. Direct Z-scheme ZnO/CdS hierarchical photocatalyst for enhanced photocatalytic H2-production activity. *Appl. Catal. B Environ.* **2019**, *243*, 19–26. [CrossRef]
114. She, X.; Wu, J.; Zhong, J.; Xu, H.; Yang, Y.; Vajtai, R.; Lou, J.; Liu, Y.; Du, D.; Li, H.; et al. Oxygenated monolayer carbon nitride for excellent photocatalytic hydrogen evolution and external quantum efficiency. *Nano Energy* **2016**, *27*, 138–146. [CrossRef]
115. Zhang, J.; Hu, Y.; Jiang, X.; Chen, S.; Meng, S.; Fu, X. Design of a direct Z-scheme photocatalyst: Preparation and characterization of Bi_2O_3/g-C3N4 with high visible light activity. *J. Hazard. Mater.* **2014**, *280*, 713–722. [CrossRef] [PubMed]
116. Li, X.; Xie, K.; Song, L.; Zhao, M.; Zhang, Z. Enhanced Photocarrier Separation in Hierarchical Graphitic-C_3N_4-Supported $CuInS_2$ for Noble-Metal-Free Z-Scheme Photocatalytic Water Splitting. *ACS Appl. Mater. Interfaces* **2017**, *9*, 24577–24583. [CrossRef]
117. Lv, S.; Wang, Y.; Zhou, Y.; Liu, Q.; Song, C.; Wang, D. Oxygen vacancy stimulated direct Z-scheme of mesoporous Cu_2O/TiO_2 for enhanced photocatalytic hydrogen production from water and seawater. *J. Alloys Compd.* **2021**, *868*. [CrossRef]
118. Ohno, T.; Murakami, N.; Koyanagi, T.; Yang, Y. Photocatalytic reduction of CO_2 over a hybrid photocatalyst composed of WO_3 and graphitic carbon nitride (g-C_3N_4) under visible light. *J. CO2 Util.* **2014**, *6*, 17–25. [CrossRef]
119. Liu, Y.; Zheng, X.; Yang, Y.; Li, J.; Liu, W.; Shen, Y.; Tian, X. Photocatalytic Hydrogen Evolution Using Ternary-Metal-Sulfide/TiO_2 Heterojunction Photocatalysts. *ChemCatChem* **2022**, *14*, e202101439. [CrossRef]
120. Li, Z.; Luan, Y.; Qu, Y.; Jing, L. Modification Strategies with Inorganic Acids for Efficient Photocatalysts by Promoting the Adsorption of O_2. *ACS Appl. Mater. Interfaces* **2015**, *7*, 22727–22740. [CrossRef]
121. Cui, H.; Cao, Y.; Jing, L.; Luan, Y.; Li, N. Effects of Inorganic Acid Modification on Photocatalytic Performance of TiO_2 and Its Activity-Enhanced Mechanism Related to Adsorbed O_2. *ChemPlusChem* **2013**, *79*, 318–324. [CrossRef]

122. Cao, Y.; Jing, L.; Shi, X.; Luan, Y.; Durrant, J.R.; Tang, J.; Fu, H. Enhanced photocatalytic activity of nc-TiO_2 by promoting photogenerated electrons captured by the adsorbed oxygen. *Phys. Chem. Chem. Phys.* **2012**, *14*, 8530–8536. [CrossRef]
123. Montoya, A.T.; Gillan, E.G. Enhanced Photocatalytic Hydrogen Evolution from Transition-Metal Surface-Modified TiO_2. *ACS Omega* **2018**, *34*, 2947–2955. [CrossRef]
124. Li, L.; Rohrer, G.S.; Salvador, P.A.; Dickey, E. Heterostructured Ceramic Powders for Photocatalytic Hydrogen Production: Nanostructured TiO_2 Shells Surrounding Microcrystalline (Ba,Sr) TiO_3 Cores. *J. Am. Ceram. Soc.* **2012**, *95*, 1414–1420. [CrossRef]
125. Zhang, W.; Wang, S.; Li, J.; Yang, X. Photocatalytic hydrogen production from methanol aqueous solution under visible-light using Cu/S–TiO2 prepared by electroless plating method. *Catal. Commun.* **2015**, *59*, 189–194. [CrossRef]
126. Jing, D.; Zhang, Y.; Guo, L. Study on the synthesis of Ni doped mesoporous TiO2 and its photocatalytic activity for hydrogen evolution in aqueous methanol solution. *Chem. Phys. Lett.* **2005**, *415*, 74–78. [CrossRef]
127. Zhao, W.; Wang, X.; Sang, H.; Wang, K. Synthesis of Bi-doped TiO_2 Nanotubes and Enhanced Photocatalytic Activity for Hydrogen Evolution from Glycerol Solution. *Chin. J. Chem.* **2013**, *31*, 415–420. [CrossRef]
128. Kong, X.; Peng, Z.; Jiang, R.; Jia, P.; Feng, J.; Yang, P.; Chi, Q.; Ye, W.; Xu, F.; Gao, P. Nanolayered Heterostructures of N-Doped TiO2, and N-Doped Carbon for Hydrogen Evolution. *ACS Appl. Nano Mater.* **2020**, *3*, 1373–1381. [CrossRef]
129. Sayed, F.N.; Jayakumar, O.D.; Sasikala, R.; Kadam, R.M.; Bharadwaj, S.R.; Kienle, L.; Schürmann, U.; Kaps, S.; Adelung, R.; Mittal, J.P.; et al. Photochemical Hydrogen Generation Using Nitrogen-Doped TiO_2–Pd Nanoparticles: Facile Synthesis and Effect of Ti^{3+} Incorporation. *J. Phys. Chem. C* **2012**, *116*, 12462–12467. [CrossRef]
130. Xing, Z.; Li, Z.; Wu, X.; Wang, G.; Zhou, W. In-situ S-doped porous anatase TiO2 nanopillars for high-efficient visible-light photocatalytic hydrogen evolution. *Int. J. Hydrogen Energy* **2016**, *41*, 1535–1541. [CrossRef]
131. Caudillo-Flores, U.; Muñoz-Batista, M.J.; Cortés, J.A.; Fernández-García, M.; Kubacka, A. UV and visible light driven H2 photo-production using Nb-doped TiO_2: Comparing Pt and Pd co-catalysts. *Mol. Catal.* **2017**, *437*, 1–10. [CrossRef]
132. Sreethawong, T.; Yoshikawa, S. Impact of photochemically deposited monometallic Pt and bimetallic Pt–Au nanoparticles on photocatalytic dye-sensitized H2 production activity of mesoporous-assembled TiO_2–SiO_2 mixed oxide nanocrystal. *Chem. Eng. J.* **2012**, *197*, 272–282. [CrossRef]
133. Wang, Q.; Xiao, L.; Liu, X.; Sun, X.; Wang, J.; Du, H. Special Z-scheme Cu_3P/TiO_2 hetero-junction for efficient photocatalytic hydrogen evolution from water. *J. Alloys Compd.* **2022**, *894*, 162331. [CrossRef]
134. Zhang, B.; Liu, F.; Sun, B.; Gao, T.; Zhou, G. Hierarchical S-scheme heterojunctions of $ZnIn_2S_4$-decorated TiO_2 for enhancing photocatalytic H2 evolution. *Chin. J. Catal.* **2024**, *59*, 334–345. [CrossRef]
135. Yu, C.; Li, M.; Yang, D.; Pan, K.; Yang, F.; Xu, Y.; Yuan, L.; Qu, Y.; Zhou, W. NiO nanoparticles dotted TiO_2 nanosheets assembled nanotubes P-N heterojunctions for efficient interface charge separation and photocatalytic hydrogen evolution. *Appl. Surf. Sci.* **2021**, *568*. [CrossRef]
136. Yang, S.; Wang, K.; Chen, Q.; Wu, Y. Enhanced photocatalytic hydrogen production of S-scheme $TiO_2/g\text{-}C_3N_4$ heterojunction loaded with single-atom Ni. *J. Mater. Sci. Technol.* **2024**, *175*, 104–114. [CrossRef]
137. Liu, C.; Chen, L.; Su, X.; Chen, S.; Zhang, L.J.; Yang, H.; Pei, Y. Activating a $TiO_2/BiVO_4$ Film for Photoelectrochemical Water Splitting by Constructing a Heterojunction Interface with a Uniform Crystal Plane Orientation. *ACS Appl. Mater. Interfaces* **2022**, *14*, 2316–2325. [CrossRef]
138. Lee, M.G.; Yang, J.W.; Park, H.; Moon, C.W.; Andoshe, D.M.; Park, J.; Moon, C.-K.; Lee, T.H.; Choi, K.S.; Cheon, W.S.; et al. Crystal Facet Engineering of TiO_2 Nanostructures for Enhancing Photoelectrochemical Water Splitting with $BiVO_4$ Nanodots. *Nano-Micro Lett.* **2022**, *14*, 48. [CrossRef]
139. Chen, H.; Li, J.; Yang, W.; Balaghi, S.E.; Triana, C.A.; Mavrokefalos, C.K.; Patzke, G.R. The Role of Surface States on Reduced TiO_2@$BiVO_4$ Photoanodes: Enhanced Water Oxidation Performance through Improved Charge Transfer. *ACS Catal.* **2021**, *11*, 7637–7646. [CrossRef]
140. Chen, W.; Wang, T.; Xue, J.; Li, S.; Wang, Z.; Sun, S. Cobalt–Nickel Layered Double Hydroxides Modified on TiO_2 Nanotube Arrays for Highly Efficient and Stable PEC Water Splitting. *Small* **2017**, *13*. [CrossRef]
141. Wang, J.; Xue, C.; Yao, W.; Liu, J.; Gao, X.; Zong, R.; Yang, Z.; Jin, W.; Tao, D. MOF-derived hollow TiO2@C/FeTiO3 nanoparticles as photoanodes with enhanced full spectrum light PEC activities. *Appl. Catal. B Environ.* **2019**, *250*, 369–381. [CrossRef]
142. Jung, E.S.; Basit, M.A.; Abbas, M.A.; Ali, I.; Kim, D.W.; Park, Y.M.; Bang, J.H.; Park, T.J. Improved CdS quantum dot distribution on a TiO_2 photoanode by an atomic-layer-deposited ZnS passivation layer for quantum dot-sensitized solar cells. *Sol. Energy Mater. Sol. Cells* **2020**, *218*. [CrossRef]
143. Mohamed, N.A.; Kiong, T.S.; Ismail, A.F.; Teridi, M.A.M. Novel gamma-ray enhanced TiO_2 nanoparticles photoanode for efficient photoelectrochemical (PEC) water splitting. *Appl. Surf. Sci.* **2024**, *642*, 158602. [CrossRef]